Electronic Supplementary Material (ESI) for ChemComm.

Supporting Information

Contents

Experimental procedures

General Information

Unless otherwise stated, all reactions, manipulations, work-up and purifications were performed under inert argon atmosphere using anhydrous solvents. Reagents used in this work including Me_2SiHCl, Me_2SnCl_2 and [*n*-Bu_4N][SbF_6] were obtained commercially and used as received. $R_{ind}Br$ (R_{ind} = dispiro[fluorene-9,3'-(1',1',7',7'-tetramethyl-s-hydrindacen-4'-yl], $R_{ind}Li(THF)_2$,[S1,S2] Me_3PbBr,[S3] $K[B(C_6F_5)_4]$[S4] and $Ph_3C[B(C_6F_5)_4]$[S5] were prepared following the published procedures. Anhydrous dichloromethane, hexane and toluene were collected from an SPS800 mBraun solvent purification system and stored over 3 Å molecular sieves. Other solvents, such as 1,2-$F_2C_6H_4$ or 1,2-$Cl_2C_6H_4$, were dried directly over 3 Å molecular sieves. Deuterated solvents were degassed and dried over 3 Å molecular sieves under argon.

Unless otherwise noted, NMR spectra were recorded at room temperature on Bruker Avance Neo 600 MHz spectrometers. ^{1}H, $^{13}C\{^{1}H\}$, ^{11}B, ^{19}F, $^{29}Si\{^{1}H\}$,^{119}Sn, $^{207}Pb\{^{1}H\}$ NMR spectra are reported on the δ scale (ppm) and are referenced against $SiMe_4$, $BF_3{\cdot}Et_2O$ (15% in $CDCl_3$), $CFCl_3$, Me_4Sn (90% in C_6D_6) and Me_4Pb respectively. ^{1}H and $^{13}C\{^{1}H\}$ chemical shifts are reported relative to the residual peak of the solvent ($CDHCl_2$: 5.32 ppm, for CD_2Cl_2; C_6HD_5: 7.16 ppm for C_6D_6) in the ^{1}H NMR spectra, and to the peak of the deuterated solvent (CD_2Cl_2: 53.84 ppm; C_6D_6: 128.06 ppm) in the $^{13}C\{1H\}$ NMR spectra.[S6] Assignment of the ^{1}H and $^{13}C\{^{1}H\}$ resonance signals was made in accordance with the COSY, HSQC and HMBC spectra.

The ESI HRMS spectra were measured on a Bruker Impact II spectrometer. Acetonitrile or dichloromethane/acetonitrile solutions (c =$1{\cdot}10^{-5}$ mol·L^{-1}) were injected directly into the spectrometer at a flow rate of 3 µL·min^{-1}. Nitrogen was used both as a drying gas and for nebulization with flow rates of approximately 5 L·min^{-1} and a pressure of 5 psi. Pressure in the mass analyzer region was usually about $1{\cdot}10^{-5}$ mbar. Spectra were collected for 1 min and averaged. The nozzle-skimmer voltage was adjusted individually for each measurement. The IR spectrum was recorded on a *Nicolet* Thermo iS10 scientific spectrometer with a diamond ATR unit.

Synthesis and characterization of $R_{ind}SiMe_2H$ (2)

To a suspension of $R_{ind}Li(THF)_2$ (300 mg, 0.451 mmol) in toluene (10 mL) was added Me_2SiHCl (0.05 mL, 42.7 mg, 0.451 mmol) at room temperature. The reaction mixture was stirred for 2 hours. The turbid reaction mixture was diluted with additional toluene (20 mL) and filtered via canula filtration to remove LiCl. The solvent of the obtained solution was evaporated and the solid product was recrystallized from boiling 1,2-difluorobenzene to obtain $R_{ind}SiMe_2H$ (**2**) (158 mg, 0.276 mmol, 61%) as a crystalline colorless solid.

^{1}H NMR (600 MHz, C_6D_6): δ = 7.49 (dt, $^3J(^1H\text{-}^1H)$ = 8 Hz, $^4J(^1H\text{-}^1H)$ = 1 Hz, 4H, H14, H21), 7.45 (s, 1H, H4), 7.20 (dt, $^3J(^1H\text{-}^1H)$ = 7 Hz, $^4J(^1H\text{-}^1H)$ = 1 Hz, 4H, H11, H18), 7.10 (td, $^3J(^1H\text{-}^1H)$ = 7 Hz, $^4J(^1H\text{-}^1H)$ = 1 Hz, 4H, H13, H20), 7.03 (td, $^3J(^1H\text{-}^1H)$ = 7 Hz, $^4J(^1H\text{-}^1H)$ = 1 Hz, 4H, H12, H19), 3.06 (hept, $^1J(^1H\text{-}^{29}Si)$ = 120 Hz, $^3J(^1H\text{-}^1H)$ = 4 Hz, 1H, H24), 2.36 (s, 4H, H6a, H6b), 1.46 (s, 12H, H8, H9), −1.20 (d, $^3J(^1H\text{-}^1H)$ = 4 Hz, 6H, H22, H23). **^{13}C{^{1}H} NMR (151 MHz, CD_2Cl_2):** δ = 157.32 (s, C10, C17), 156.18 (s, C3), 150.06 (s, C2), 140.27 (s, C15, C16), 134.25 (s, C1), 127.95 (s, C12, C19), 127.11 (s, C13, C20), 124.83 (s, C11, C18), 120.43 (s, C14, C21), 119.49 (s, C4), 65.78 (s, C5), 59.81 (s, C6), 42.66 (s, C7), 32.84 (s, C8, C9), −4.63 (s, $^1J(^{13}C\text{-}^{29}Si)$ = 51 Hz, C22, C23). **^{29}Si{^{1}H} NMR (119 MHz, C_6D_6):** δ = −24.83 (s). ATR-IR: $\tilde{\nu}_{SiH}$ = 2270 cm^{-1}.

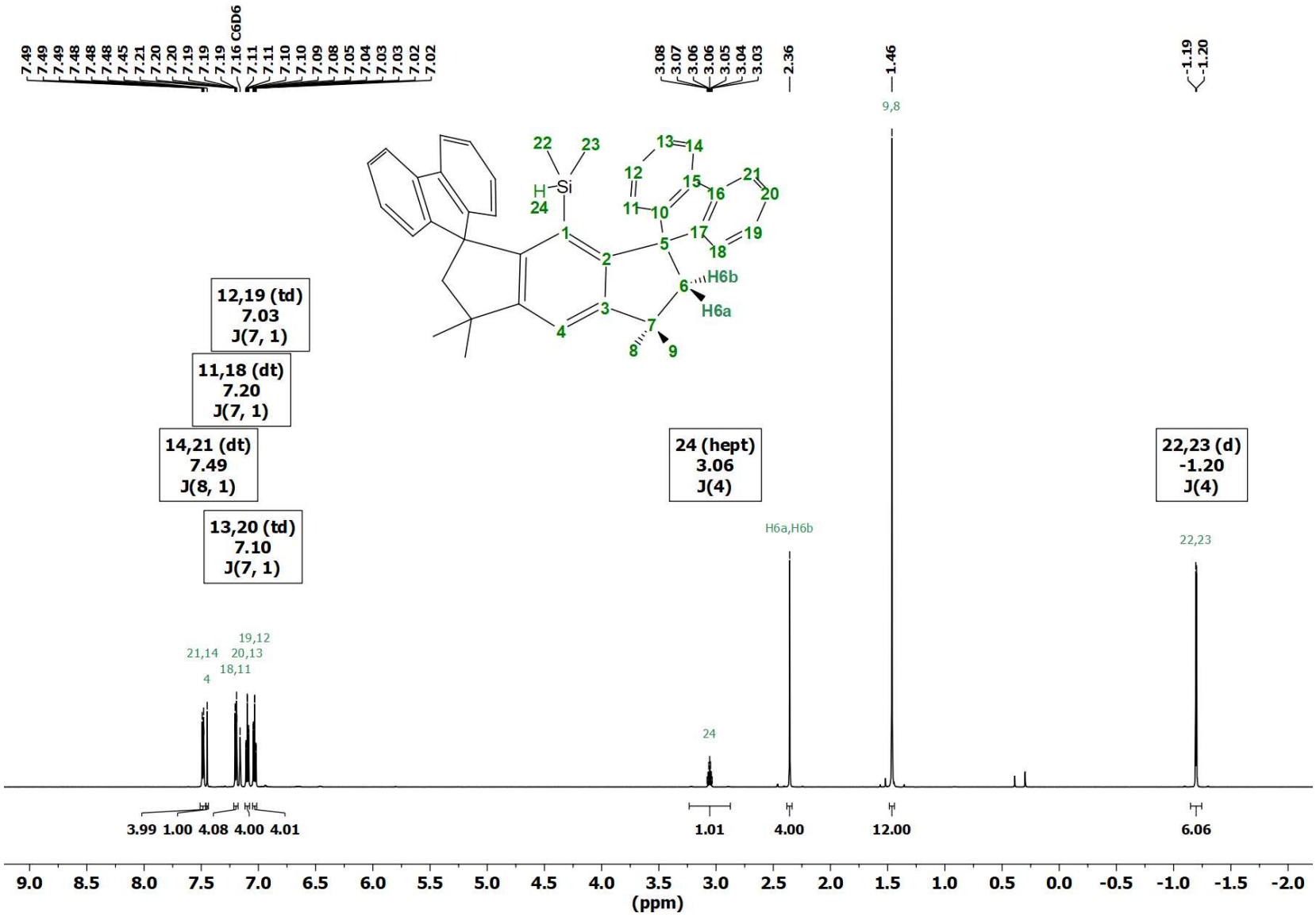

Figure S1. ^{1}H NMR (C_6D_6, 600 MHz) spectrum of **2**.

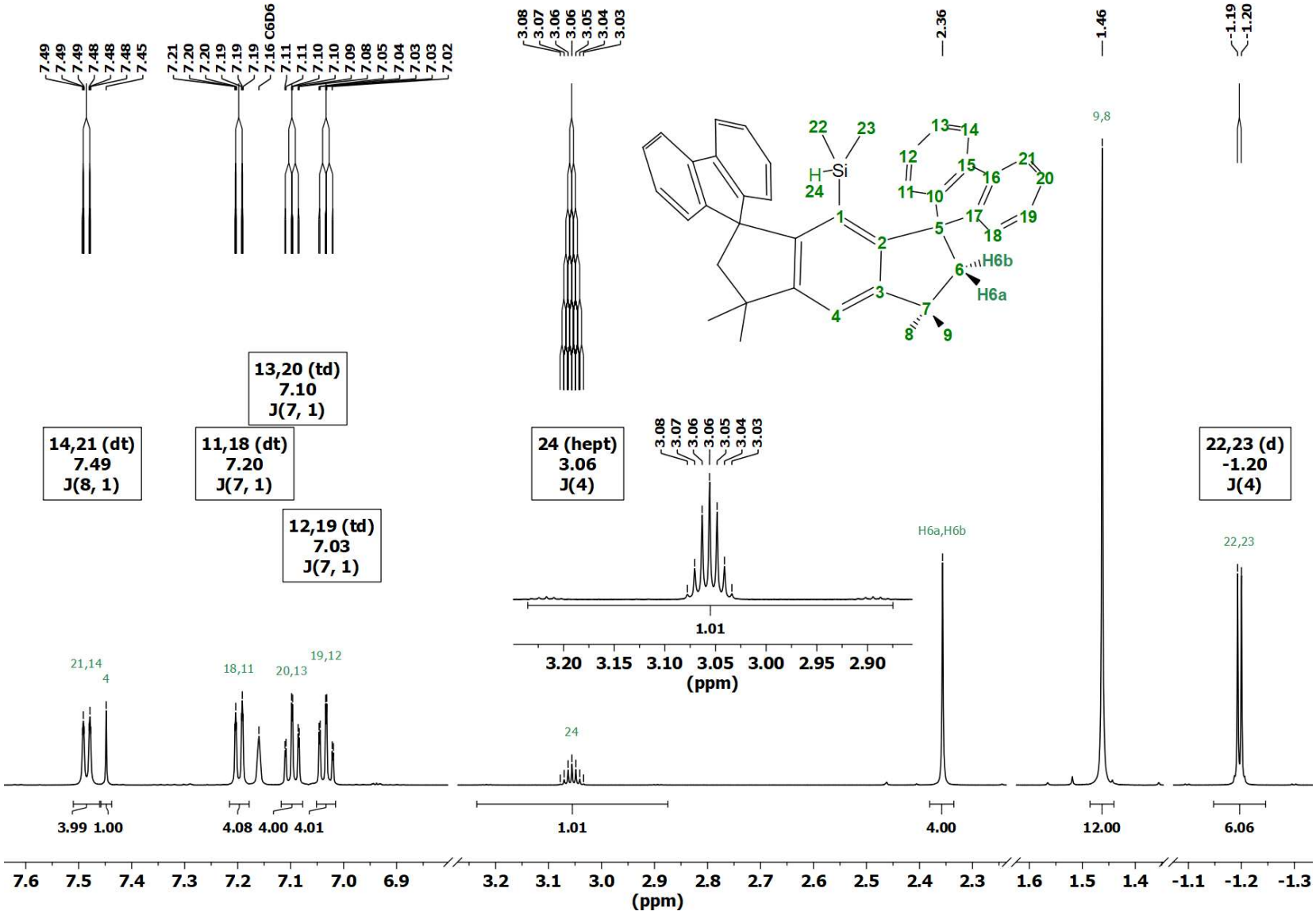

Figure S2. Detailed ^{1}H NMR (C_6D_6, 600 MHz) spectrum of **2**.

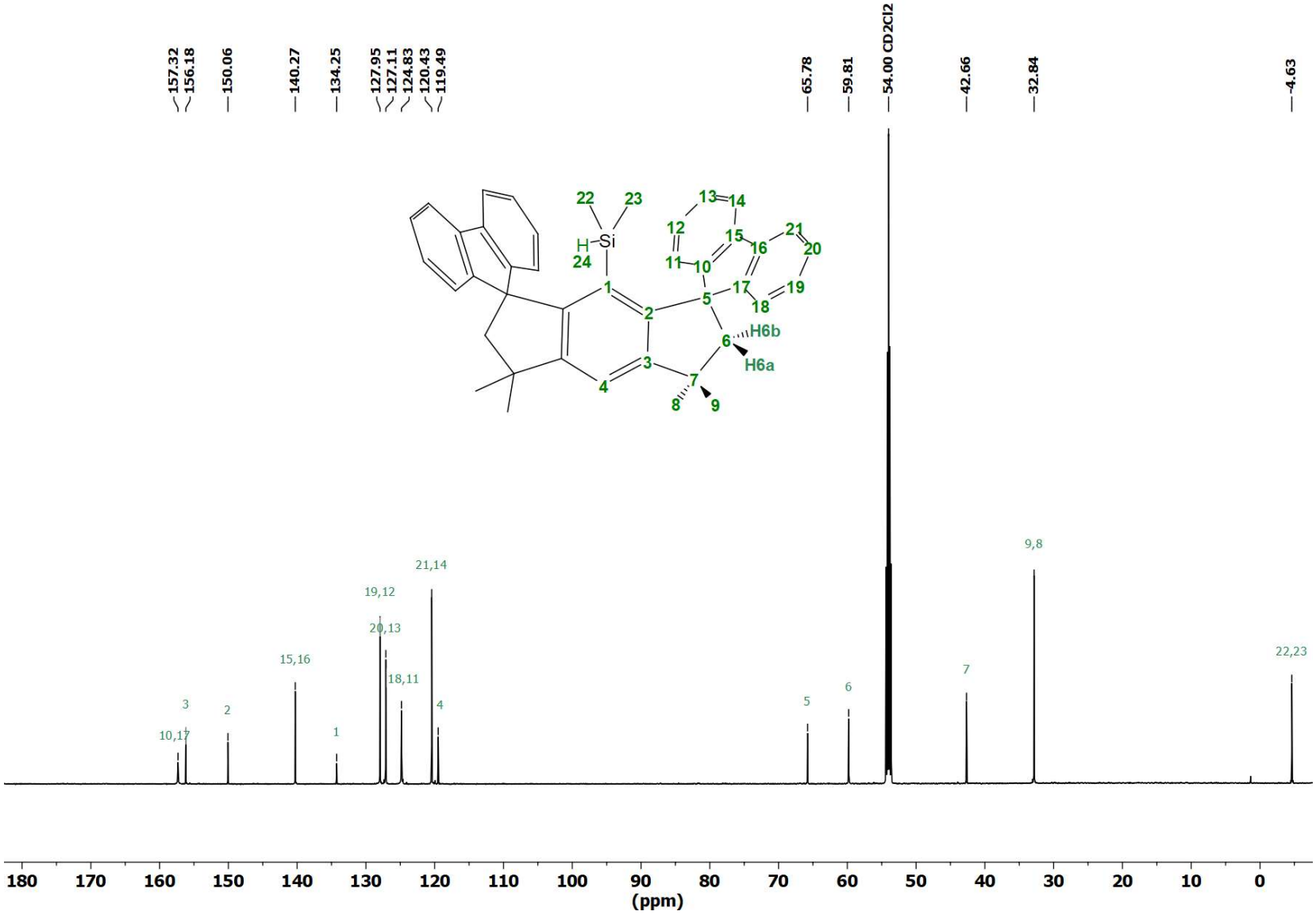

Figure S3. $^{13}C\{^{1}H\}$ NMR (CD_2Cl_2, 151 MHz) spectrum of **2**.

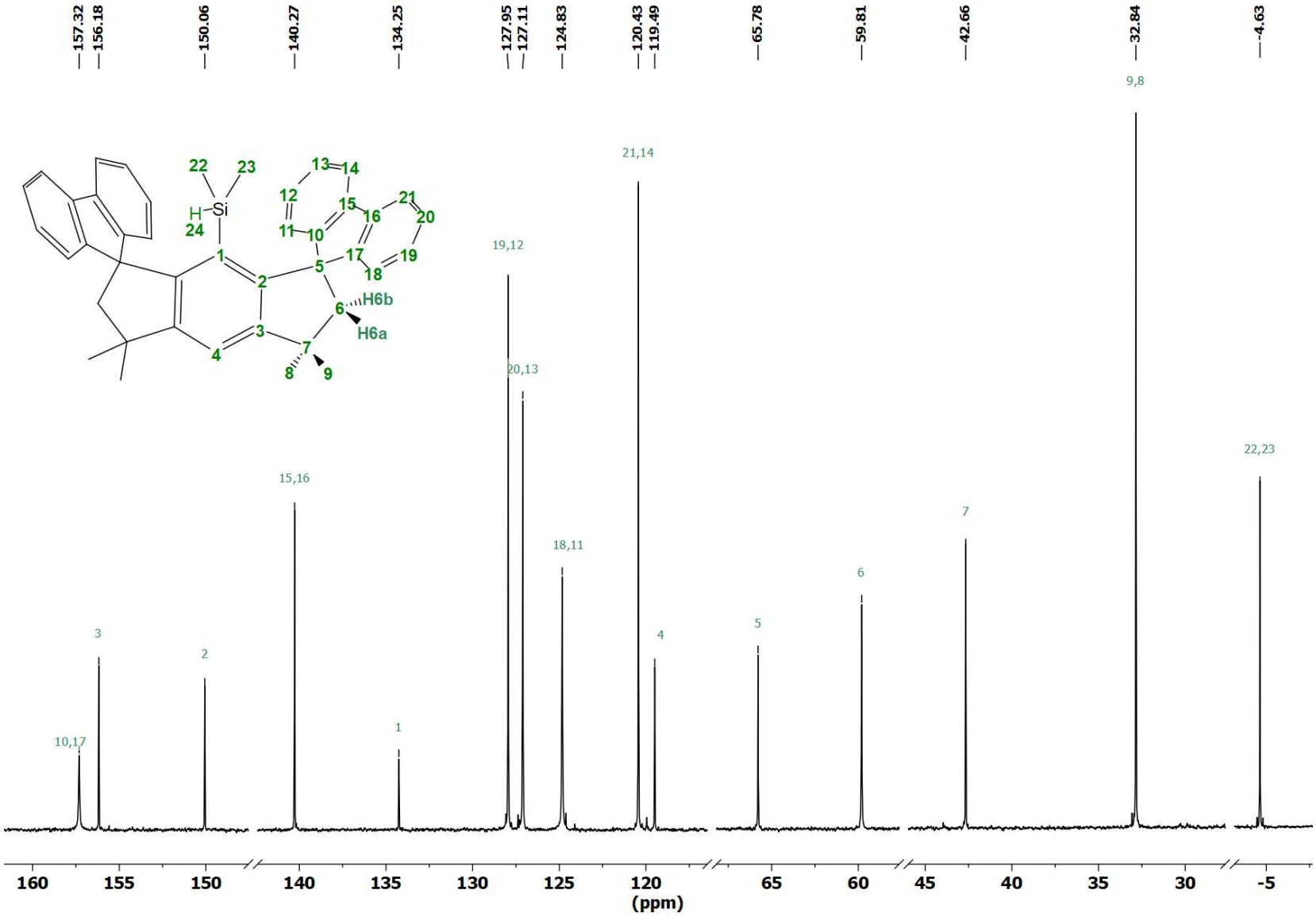

Figure S4. Detailed $^{13}C\{^{1}H\}$ NMR (CD_2Cl_2, 151 MHz) spectrum of **2**.

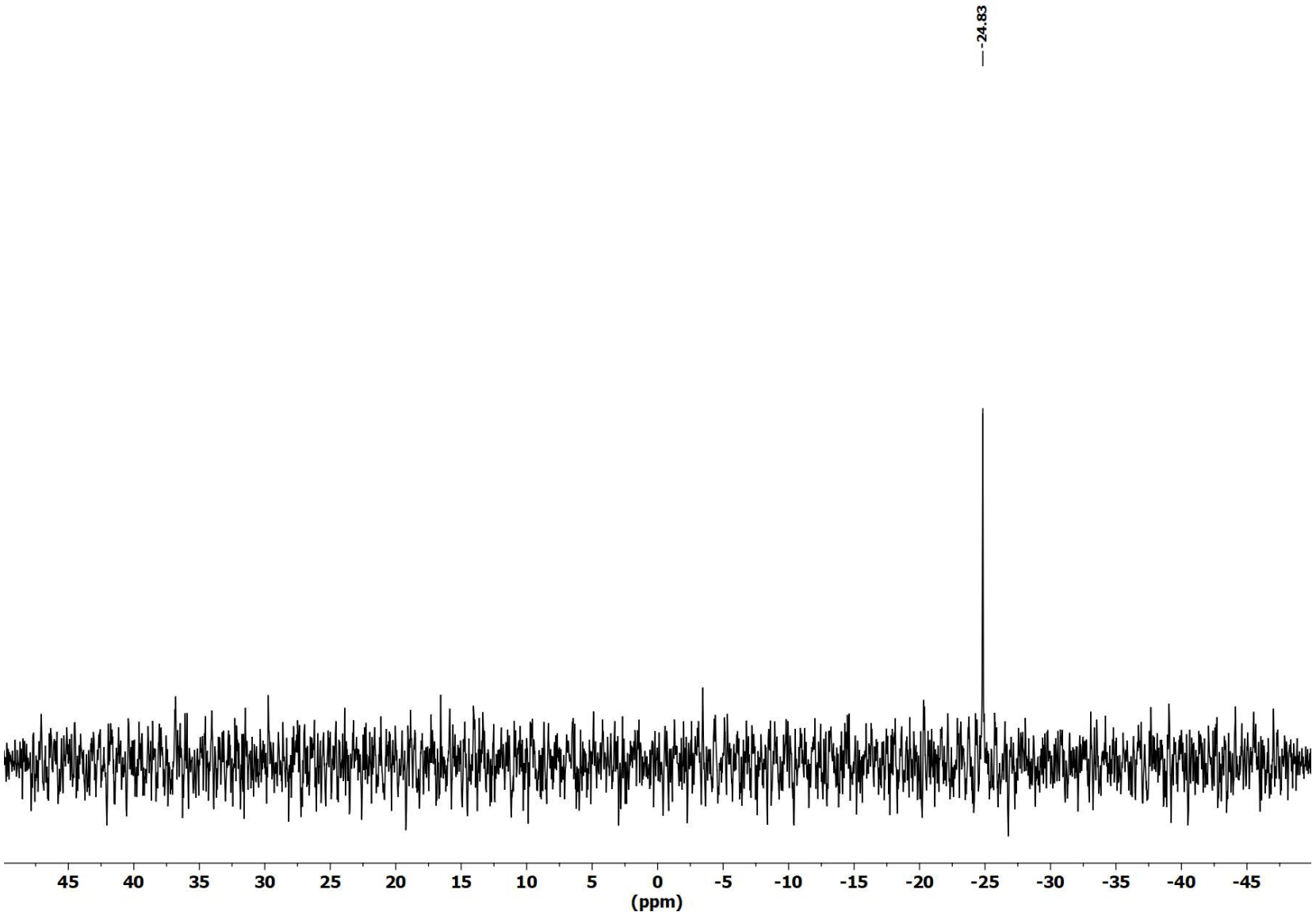

Figure S5. $^{29}Si\{^{1}H\}$ NMR (C_6D_6, 119 MHz) spectrum of **2**.

Synthesis and characterization of $R_{ind}SnMe_2Cl$ (3)

To a suspension of $R_{ind}Li(THF)_2$ (300 mg, 0.451 mmol) in toluene (10 mL) was added Me_2SnCl_2 (99.1 mg, 0.451 mmol) at room temperature. The reaction mixture was stirred for 2 hours. After evaporation of the solvent dichloromethane (20 mL) was added and the turbid solution was filtered via canula filtration to remove LiCl. The solvent was evaporated and the solid product recrystallized from boiling 1,2-difluorobenzene to obtain $R_{ind}SnMe_2Cl$ (**3**) (180 mg, 0.258 mmol, 57%) as a crystalline colorless solid.

^{1}H NMR (600 MHz, CD_2Cl_2): δ = 7.66 (ddd, $^3J(^1H\text{-}^1H)$ = 8 Hz, $^3J(^1H\text{-}^1H)$ = 1 Hz, $^4J(^1H\text{-}^1H)$ = 1 Hz, 4H, H14, H21), 7.47 (s, $^5J(^1H\text{-}^{119}Sn)$ = 10 Hz, 1H, H4), 7.29 (td, $^3J(^1H\text{-}^1H)$ = 7 Hz, $^4J(^1H\text{-}^1H)$ = 1 Hz, 4H, H13,H20), 7.22 (td, $^3J(^1H\text{-}^1H)$ = 7 Hz, $^4J(^1H\text{-}^1H)$ = 1 Hz, 4H, H12, H19), 7.19 (ddd, $^3J(^1H\text{-}^1H)$ = 8 Hz, $^3J(^1H\text{-}^1H)$ = 1 Hz, $^4J(^1H\text{-}^1H)$ = 1 Hz, 4H, H11, H18), 2.27 (s, 4H, H6a, H6b), 1.52 (s, 12H, H8, H9), −0.82 (s, $^2J(^1H\text{-}^{117/119}Sn)$ = 59/62 Hz, 6H, H22, H23). **^{13}C{^{1}H} NMR (151 MHz, CD_2Cl_2):** δ = 157.23 (s, $^3J(^{13}C\text{-}^{119}Sn)$ = 48 Hz, C3), 155.39 (s, C10, C17), 149.56 (s, $^2J(^{13}C\text{-}^{119}Sn)$ = 35 Hz, C2), 141.35 (s, C15, C16), 136.67 (s, $^1J(^{13}C\text{-}^{117/119}Sn)$ = 492/515 Hz, C1), 127.95 (s, C12, C19), 127.80 (s, C13, C20), 124.72 (s, C11, C18), 121.06 (s, C14, C21), 120.81 (s, C4), 66.70 (s, C5), 62.43 (s, C6), 42.82 (s, C7), 32.33 (s, C8, C9), 6.03 (s, $^1J(^{13}C\text{-}^{117/119}Sn)$ = 387/396 Hz, C22, C23). **^{119}Sn NMR (224 MHz, CD_2Cl_2):** δ = 49.04 (hept, $^2J(^{119}Sn\text{-}^1H)$ = 57 Hz). **HRMS ESI (m/z):** $[M-Cl]^+$ calculated for $C_{42}H_{39}Sn$, 663.20771; found 663.20710.

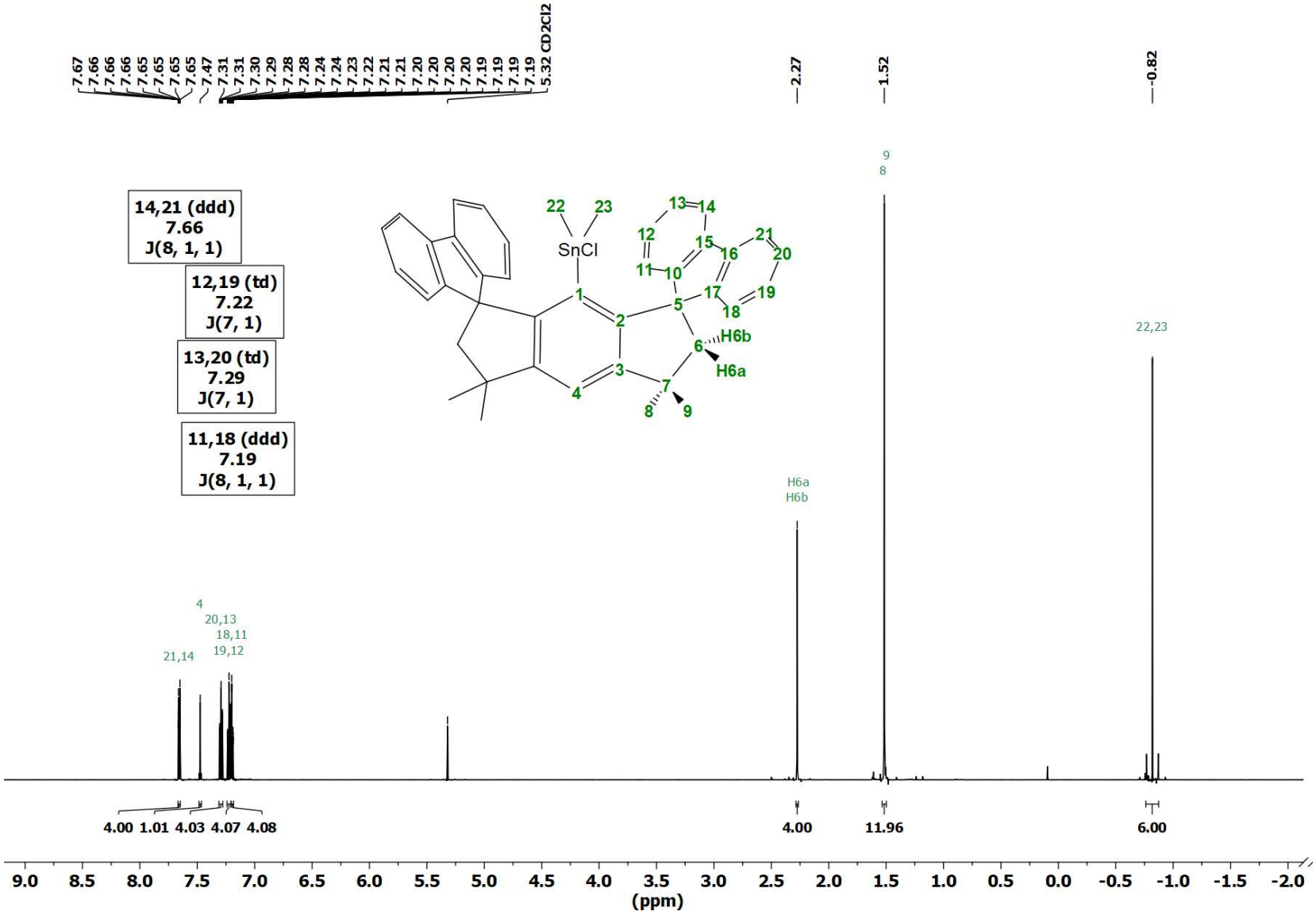

Figure S6. ^{1}H NMR (CD_2Cl_2, 600 MHz) spectrum of **3**.

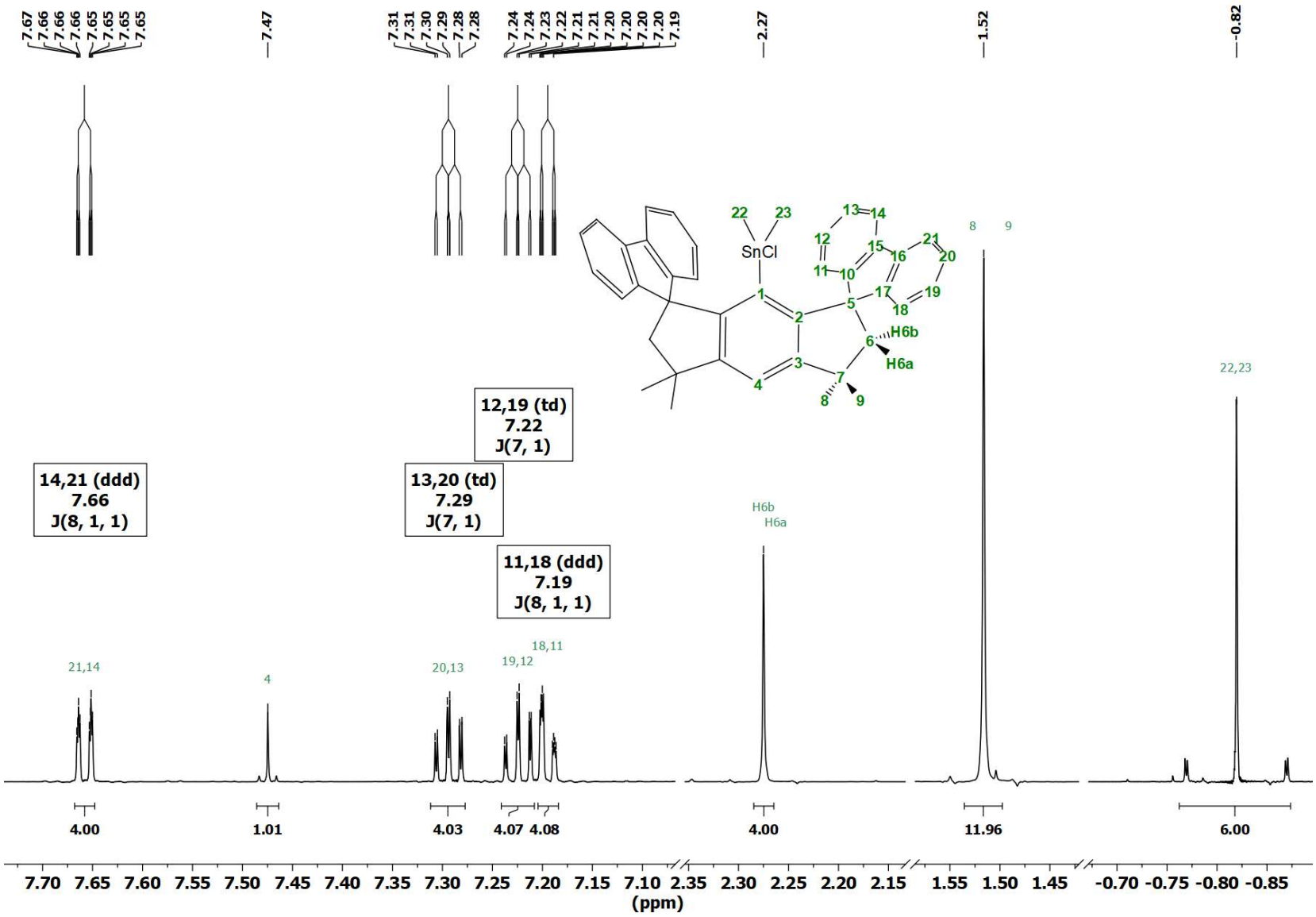

Figure S7. Detailed ^{1}H NMR (CD_2Cl_2, 600 MHz) spectrum of **3**.

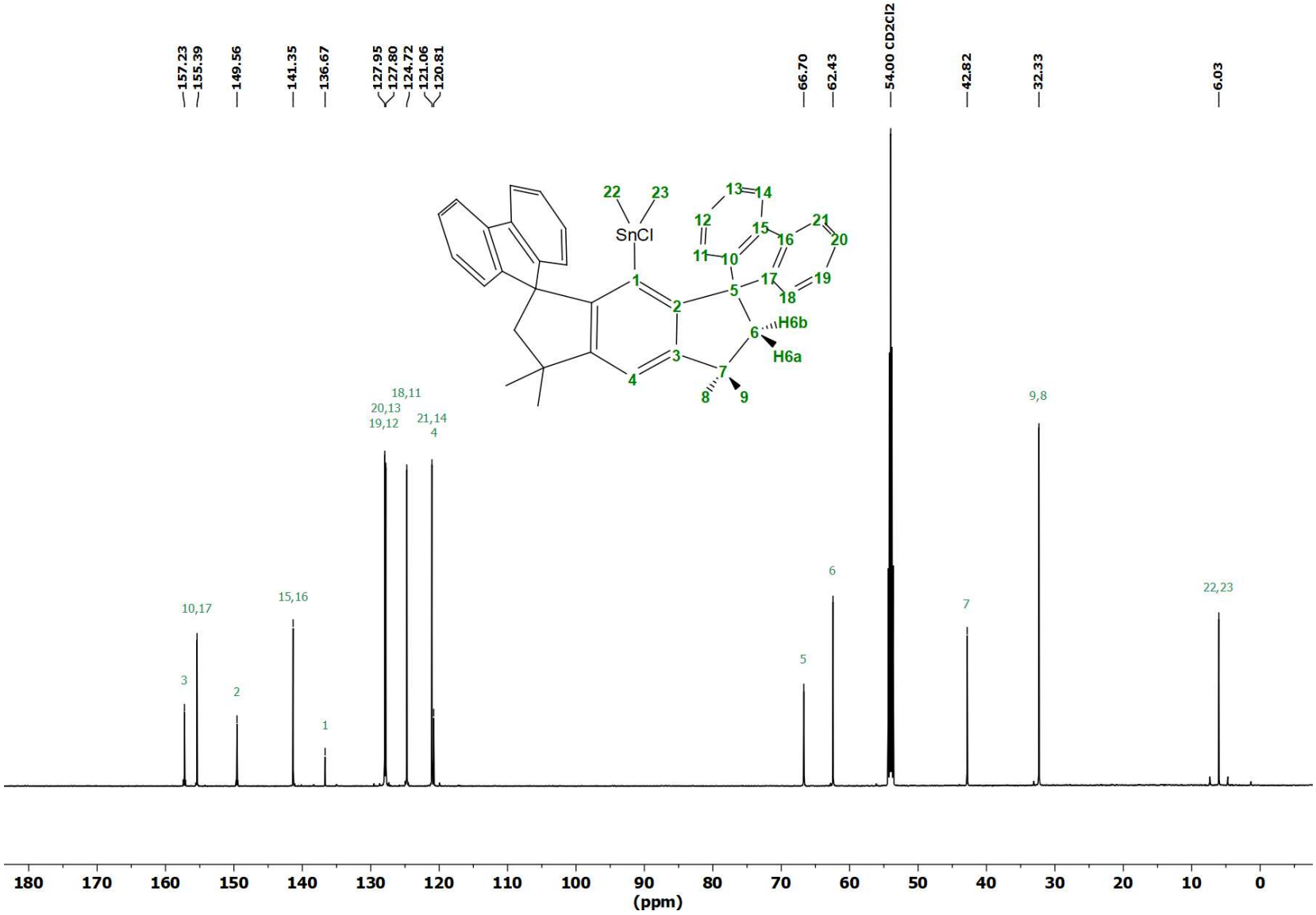

Figure S8. $^{13}C\{^{1}H\}$ NMR (CD_2Cl_2, 151 MHz) spectrum of **3**.

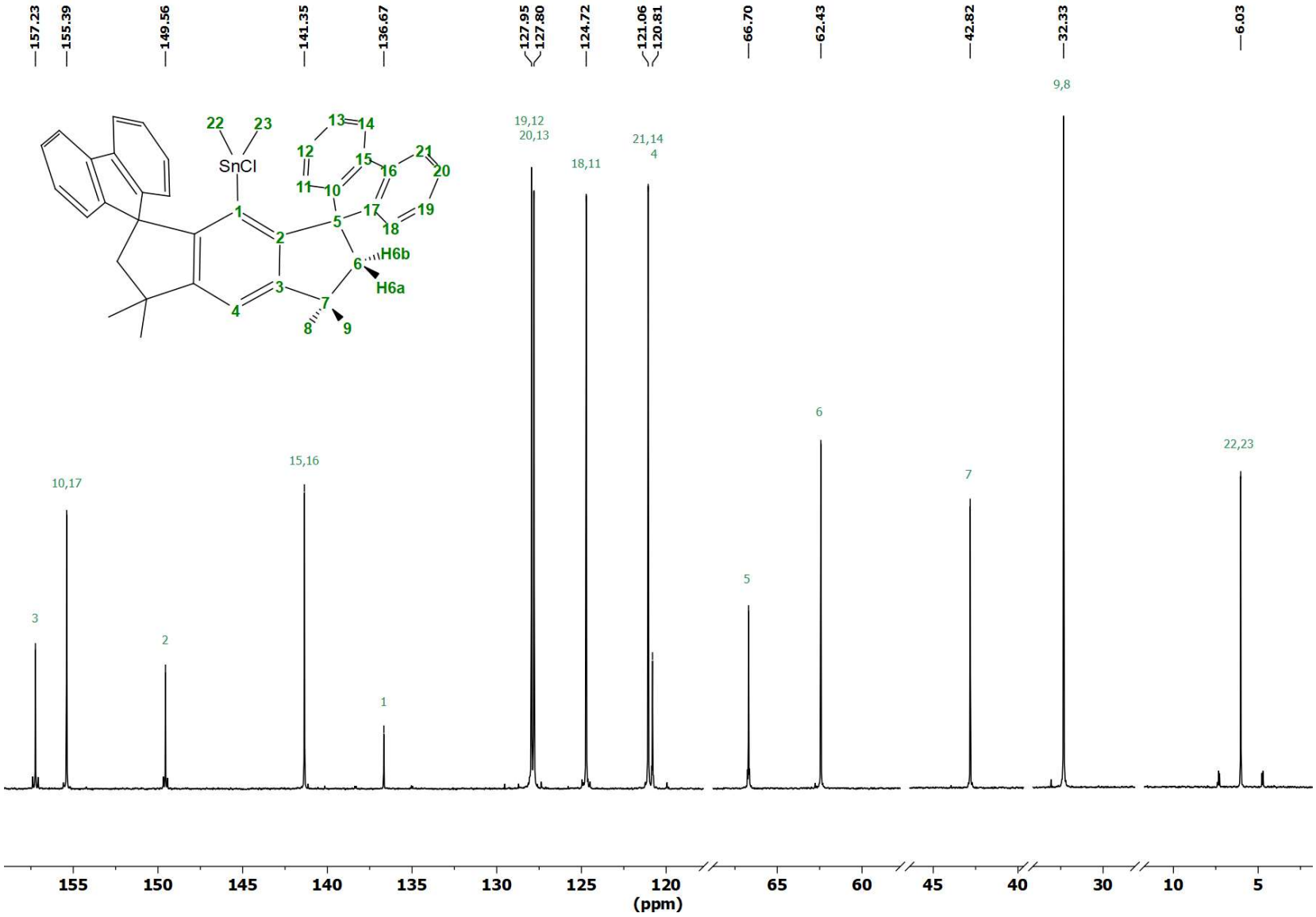

Figure S9. Detailed $^{13}C\{^{1}H\}$ NMR (CD_2Cl_2, 151 MHz) spectrum of **3**.

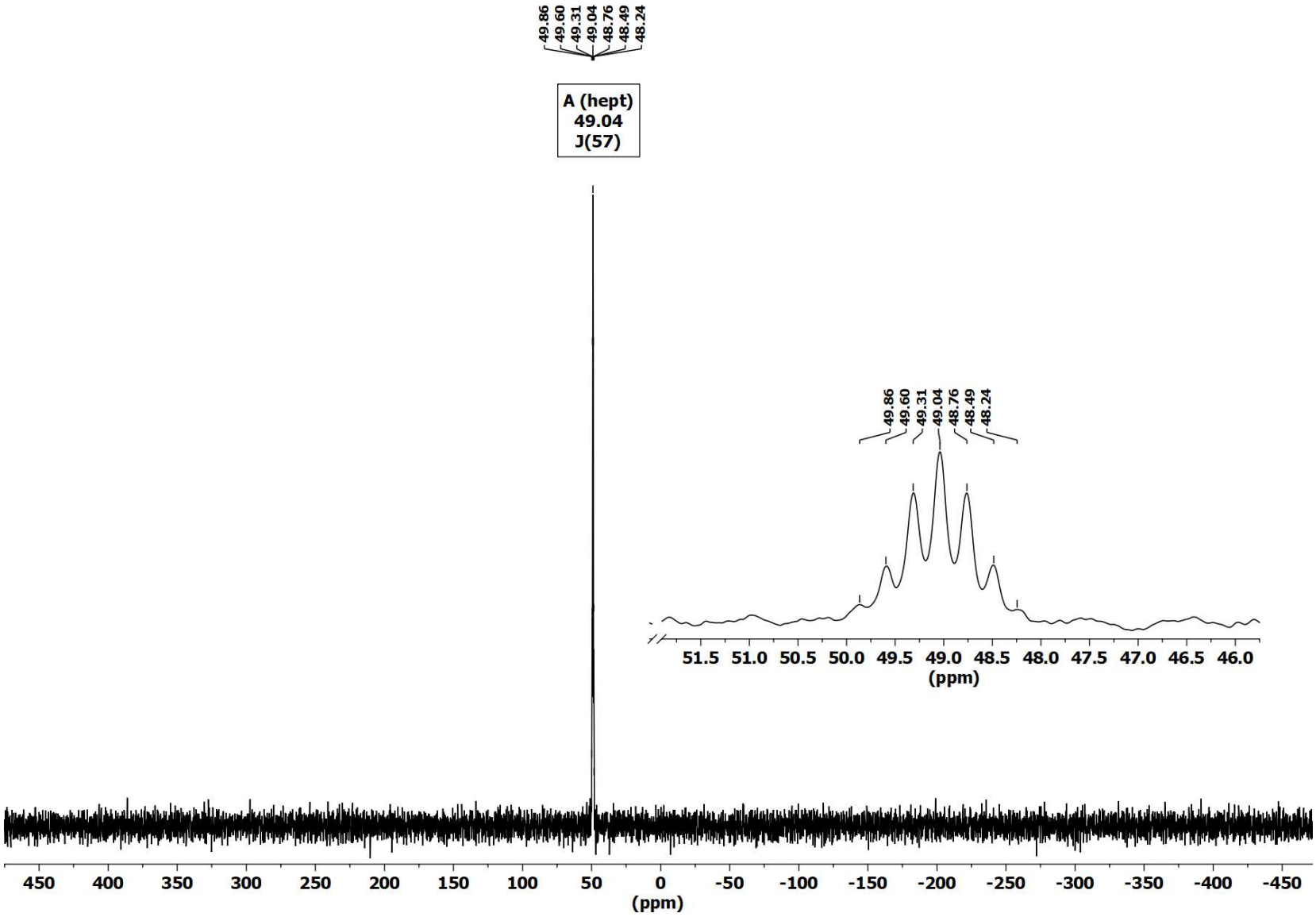

Figure S10. ^{119}Sn NMR (CD_2Cl_2, 224 MHz) spectrum of **3**.

Synthesis and characterization of $R_{ind}PbMe_3$ (4)

$R_{ind}Li(THF)_2$ (300 mg, 0.451 mmol) and Me_3PbBr (150 mg, 0.451 mmol) were suspended in toluene (15 mL) and stirred for 2 hours at room temperature. The turbid reaction mixture was diluted with additional toluene (20 mL) and filtered via canula filtration to remove LiCl. The solvent of the obtained solution was removed under reduced pressure to give $R_{ind}PbMe_3$ (**4**) as a pale yellow solid (247 mg, 0.322 mmol, 71%).

^{1}H NMR (600 MHz, CD_2Cl_2): δ = 7.50 (dt, $^3J(^1H\text{-}^1H)$ = 7 Hz, $^4J(^1H\text{-}^1H)$ = 1 Hz, 4H, H14, H21), 7.39 (s, $^5J(^1H\text{-}^{207}Pb)$ = 16 Hz, 1H, H4), 7.22 (dt, $^3J(^1H\text{-}^1H)$ = 8 Hz, $^4J(^1H\text{-}^1H)$ = 1 Hz, 4H, H11, H18), 7.12 (td, $^3J(^1H\text{-}^1H)$ = 7 Hz, $^4J(^1H\text{-}^1H)$ = 1 Hz, 4H, H13, H20), 7.05 (td, $^3J(^1H\text{-}^1H)$ = 7 Hz, $^4J(^1H\text{-}^1H)$ = 1 Hz, 4H, H12, H19)), 2.27 (s, 4H, H6a, H6b), 1.43 (s, 12H, H8, H9), −0.31 (s, $^2J(^1H\text{-}^{207}Pb)$ = 62 Hz, 9H, H22, H23 and H24). **^{13}C{^{1}H} NMR (151 MHz, CD_2Cl_2):** δ = 156.50 (s, C3), 156.04 (s, C10, C17), 150.46 (s, C2), 145.97 (s, C1), 140.84 (s, C15, C16), 127.82 (s, C12, C19), 127.32 (s, C13, C20), 124.40 (s, C11, C18), 120.89 (s, C14, C21), 117.93 (s, C4), 67.45 (s, C5), 61.95 (s, C6), 42.39 (s, C7), 32.32 (s, C8, C9), 6.97 (s, $^1J(^{13}C\text{-}^{207}Pb)$ = 247 Hz, C22, C23 and C24).). **^{207}Pb{^{1}H} NMR (126 MHz, CD_2Cl_2):** −99.61 (s). **HRMS ESI (m/z):** $[M-Me]^+$ calculated for $C_{42}H_{39}Pb$, 751.28186; found 751.28072.

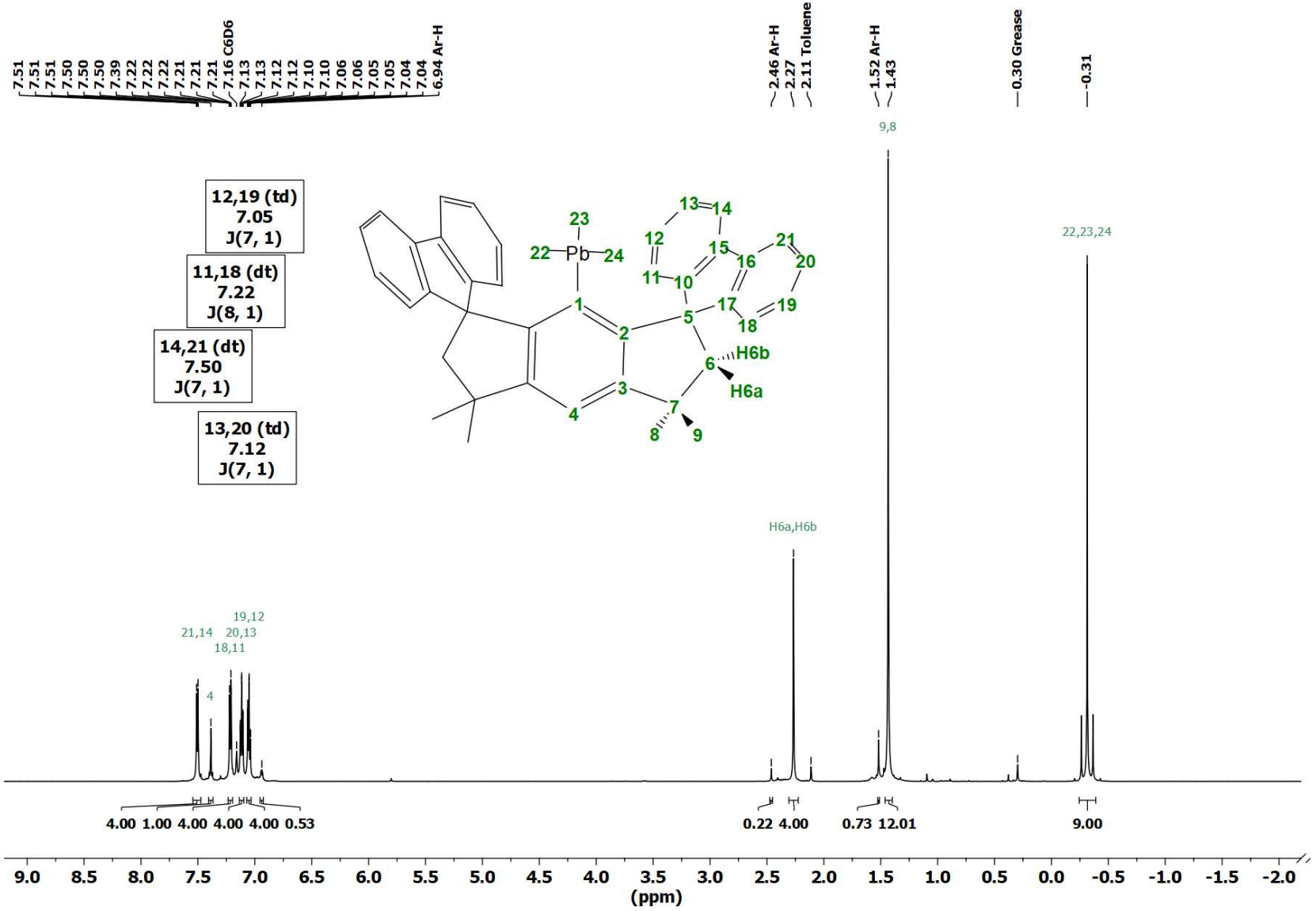

Figure S11. ^{1}H NMR (C_6D_6, 600 MHz) spectrum of **4**.

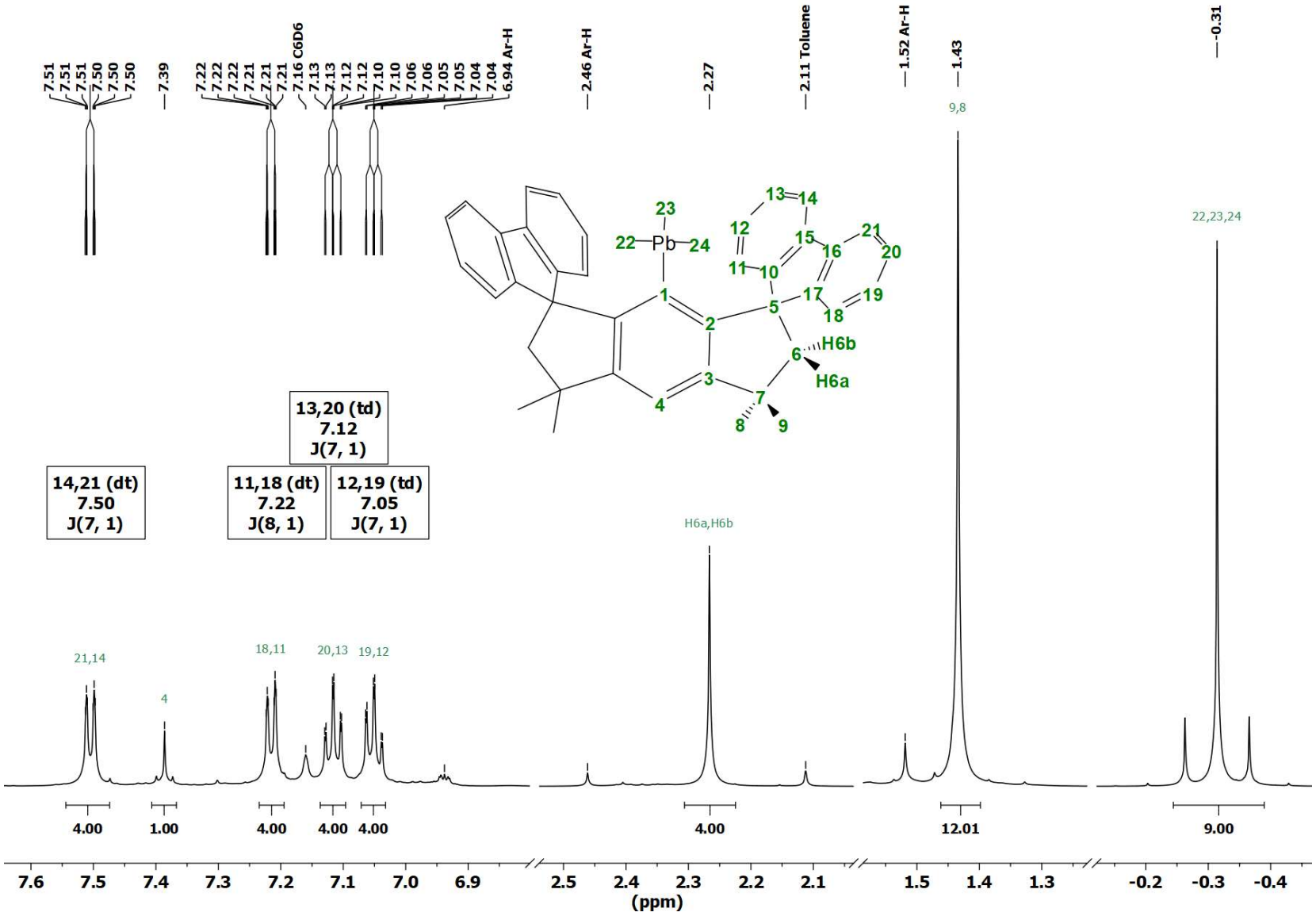

Figure S12. Detailed ^{1}H NMR (C_6D_6, 600 MHz) spectrum of **4**.

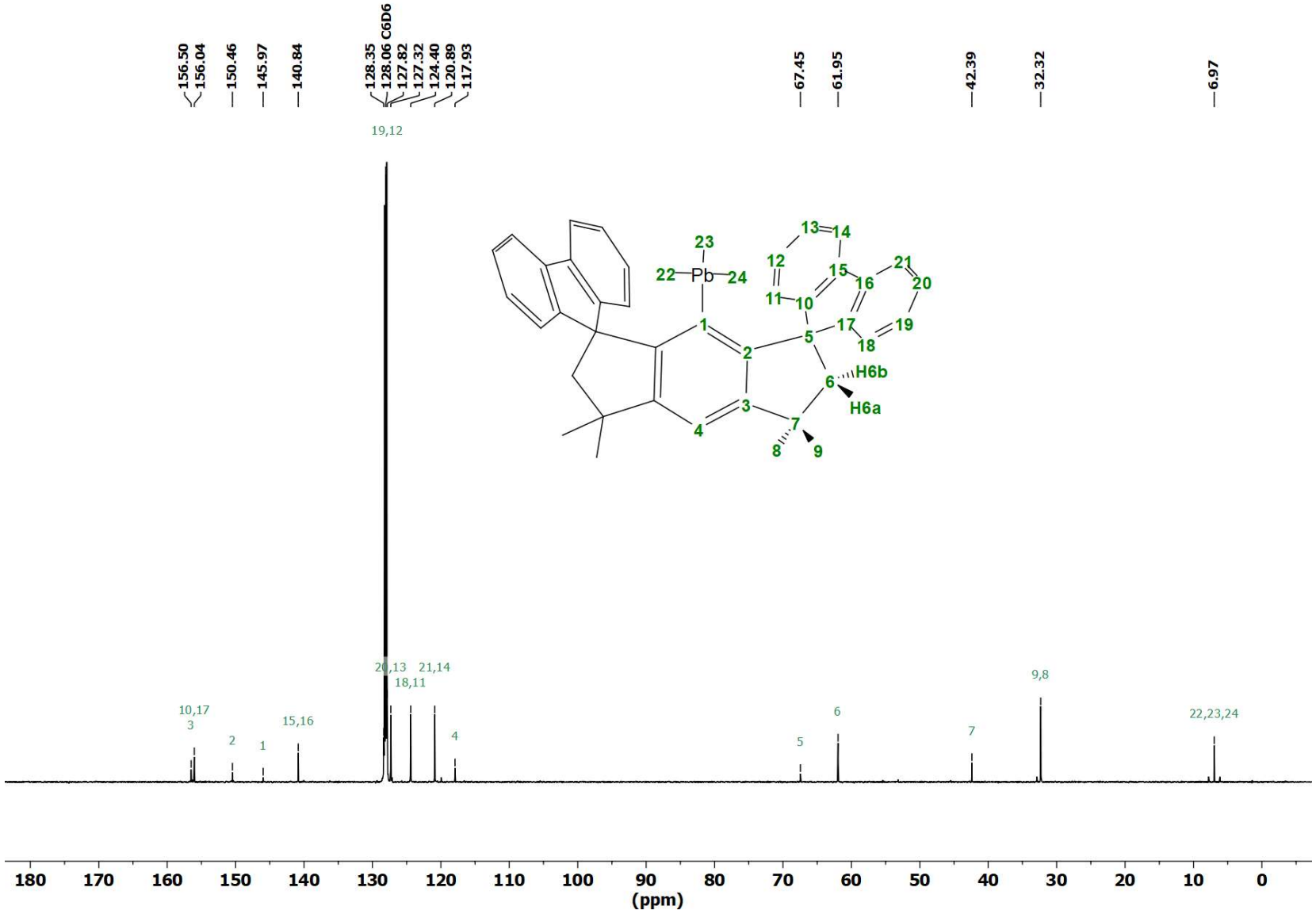

Figure S13. $^{13}C\{^{1}H\}$ NMR (CD_2Cl_2, 151 MHz) spectrum of **4**.

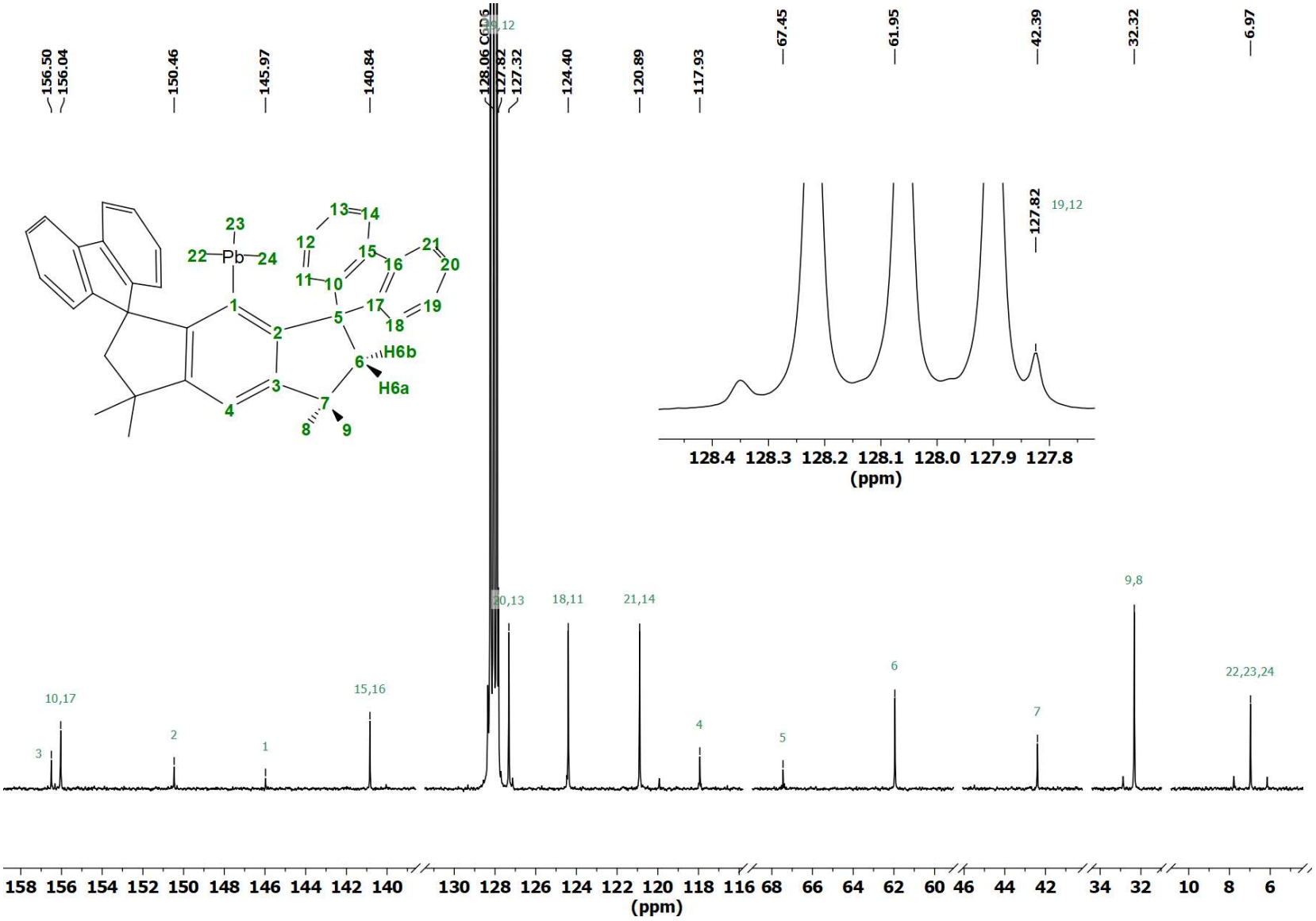

Figure S14. Detailed $^{13}C\{^{1}H\}$ NMR (CD_2Cl_2, 151 MHz) spectrum of **4**.

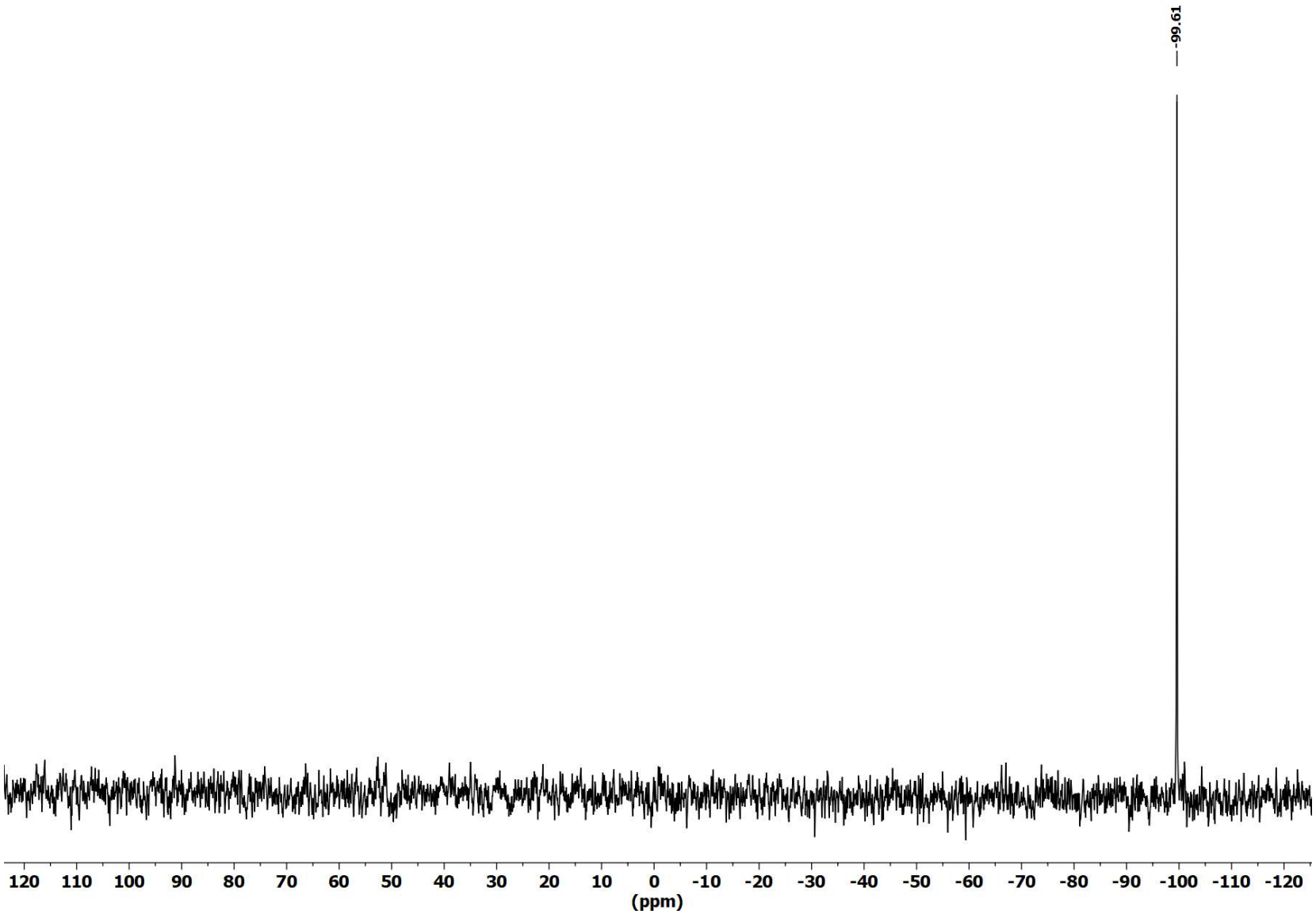

Figure S15. $^{207}Pb\{^{1}H\}$ NMR (CD_2Cl_2, 126 MHz) spectrum of **4**.

Synthesis and characterization of [$R_{ind}SiMe_2$][$B(C_6F_5)_4$] (1Si)

To a solid mixture of $R_{ind}SiMe_2H$ (**2**) (50 mg, 0.087 mmol) and $Ph_3C[B(C_6F_5)_4]$ (80.5 mg, 0.087 mmol) was added 1,2-$Cl_2C_6H_4$ (5 mL) and the reaction mixture was stirred at 85 °C for 3 days. Afterwards the reaction mixture was layered with hexane (15 mL) to obtain a yellow crystalline solid. The solid was decanted, washed with hexane (3 × 5 mL) and dried at reduced pressure to obtain [$R_{ind}SiMe_2$][$B(C_6F_5)_4$] (**1Si**) (55 mg, 0.044 mmol, 50%) as a yellow solid.

^{1}H NMR (600 MHz, CD_2Cl_2): δ = 7.69 (dt, $^3J(^1H\text{-}^1H)$ = 8 Hz, $^4J(^1H\text{-}^1H)$ = 1 Hz, 4H, H14, H21), 7.55 (s, 1H, H4), 7.48 (td, $^3J(^1H\text{-}^1H)$ = 7 Hz, $^4J(^1H\text{-}^1H)$ = 1 Hz, 4H, H13, H20), 7.35 (td, $^3J(^1H\text{-}^1H)$ = 7 Hz, $^4J(^1H\text{-}^1H)$ = 1 Hz, 4H, H12, H19), 7.30 (dt, $^3J(^1H\text{-}^1H)$ = 8 Hz, $^4J(^1H\text{-}^1H)$ = 1 Hz, 4H, H11, H18), 2.56 (s, 4H, H6a, H6b), 1.66 (s, 12H, H8, H9), −1.00 (s, $^2J(^1H\text{-}^{29}Si)$ = 128 Hz, 6H, H22, H23). **^{13}C{^{1}H} NMR (151 MHz, CD_2Cl_2):** δ = 154.77 (s, C3), 153.25 (s, C2), 151.76 (s, C10, C17), 148.71 (d, br, $^1J(^{13}C\text{–}^{19}F)$ = 242 Hz, C_6F_5), 141.26 (s, C15, C16), 138.79 (d, br, $^1J(^{13}C\text{–}^{19}F)$ = 245 Hz, C_6F_5), 136.86 (d, br, $^1J(^{13}C\text{–}^{19}F)$ = 247 Hz, C_6F_5), 132.20 (s, C13, C20), 131.61 (s, C12, C19), 128.37 (s, C11, C18), 124.03 (s, C4), 122.88 (s, C14, C21), 120.36 (s, C1), 64.43 (s, C5), 55.45 (s, C6), 45.65 (s, C7), 32.76 (s, C8, C9), 4.41 (s, C22, C23). **^{29}Si{^{1}H} NMR (119 MHz, CD_2Cl_2):** δ = 160.40 (s). **^{11}B NMR (193 MHz, CD_2Cl_2):** δ = −16.65 (s). **^{19}F NMR (565 MHz, CD_2Cl_2):** δ = −133.07 (br, 8F, *o*-C_6F_5), −163.65 (t, $^3J(^{19}F\text{-}^{19}F)$ = 20 Hz, 4F, *p*-C_6F_5), −167.50 (t, br, $^3J(^{19}F\text{-}^{19}F)$ = 19 Hz, 8F, *m*-C_6F_5).

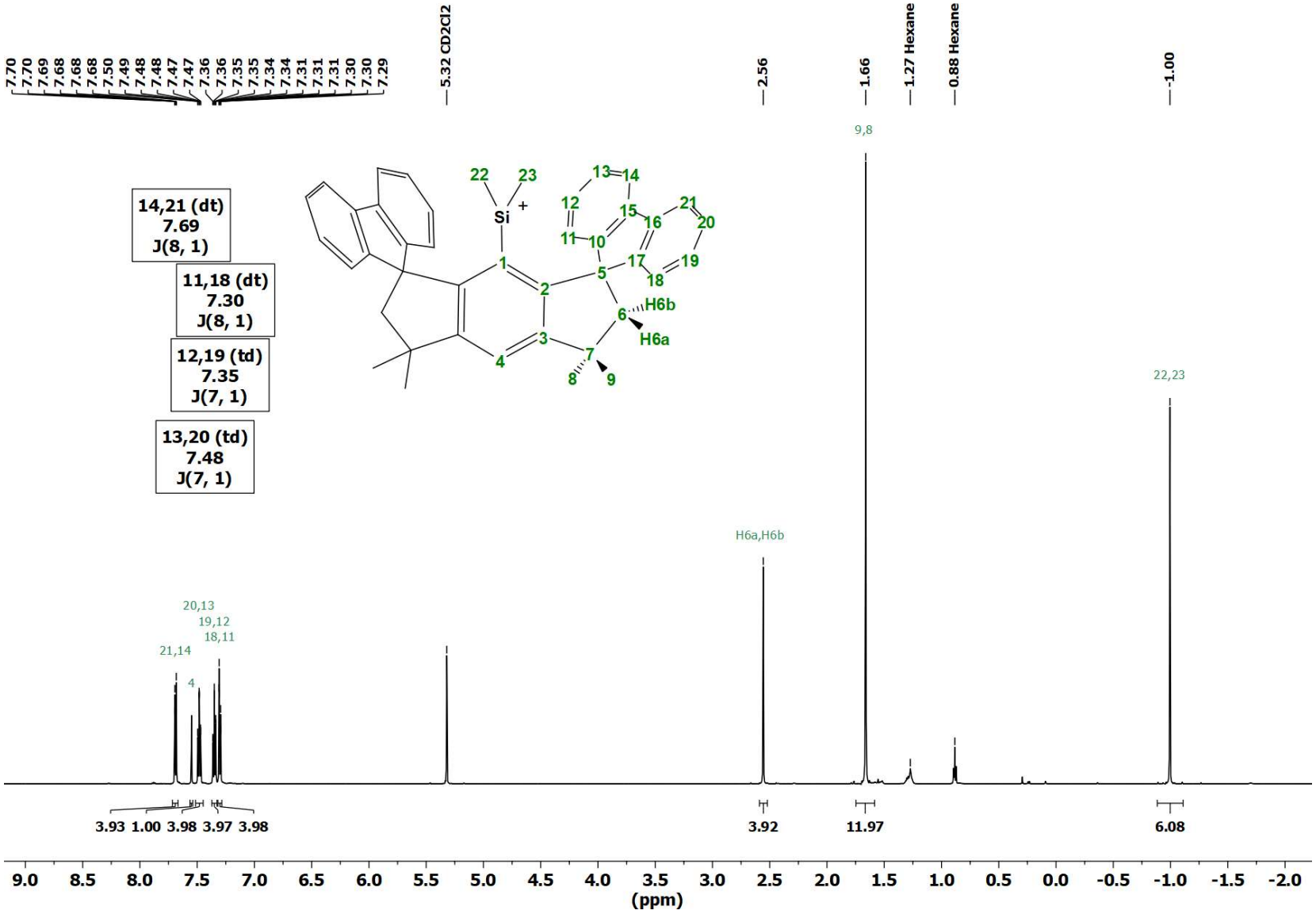

Figure S16. ^{1}H NMR (CD_2Cl_2, 600 MHz) spectrum of **1Si**.

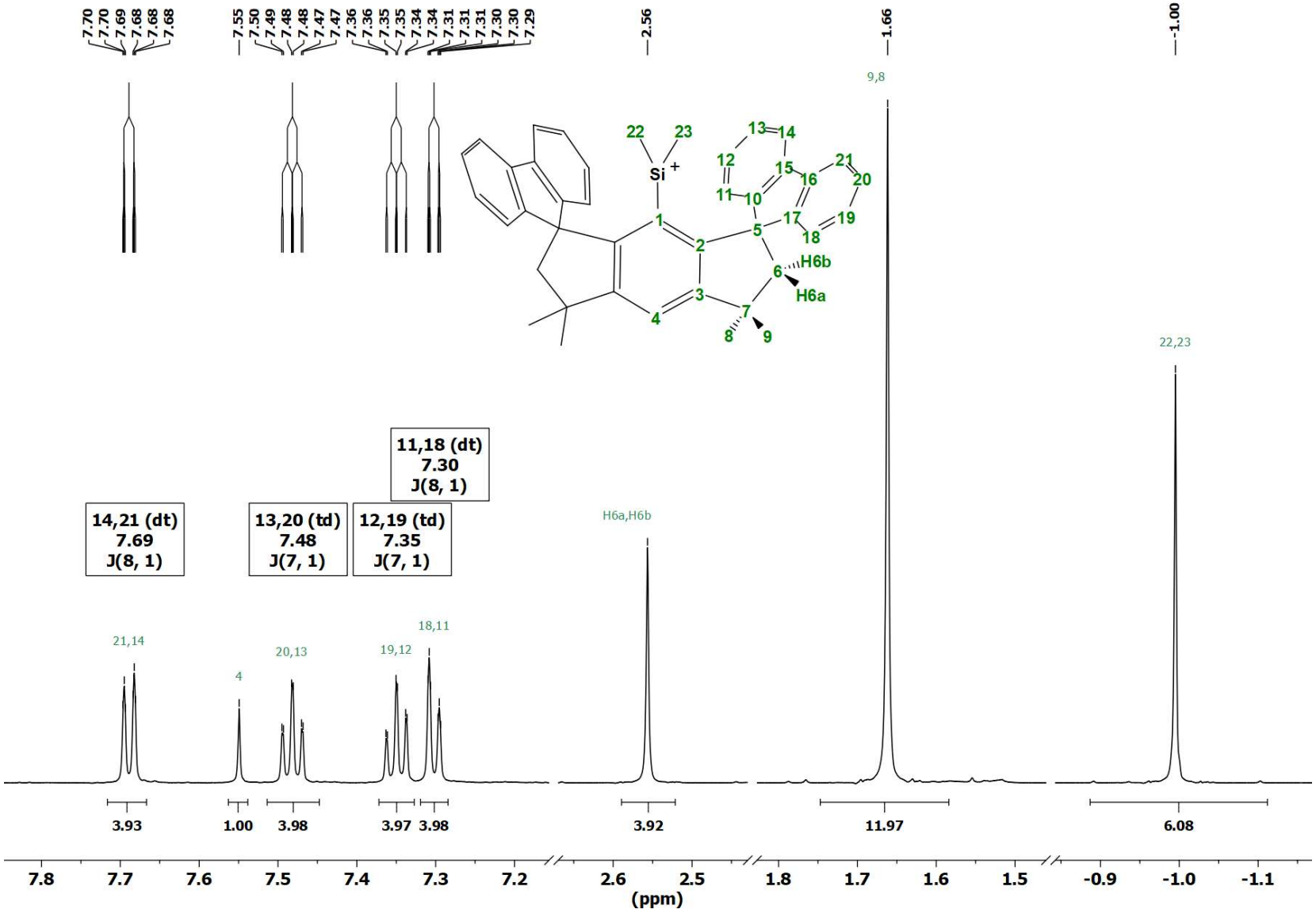

Figure S17. Detailed ^{1}H NMR (CD_2Cl_2, 600 MHz) spectrum of **1Si**.

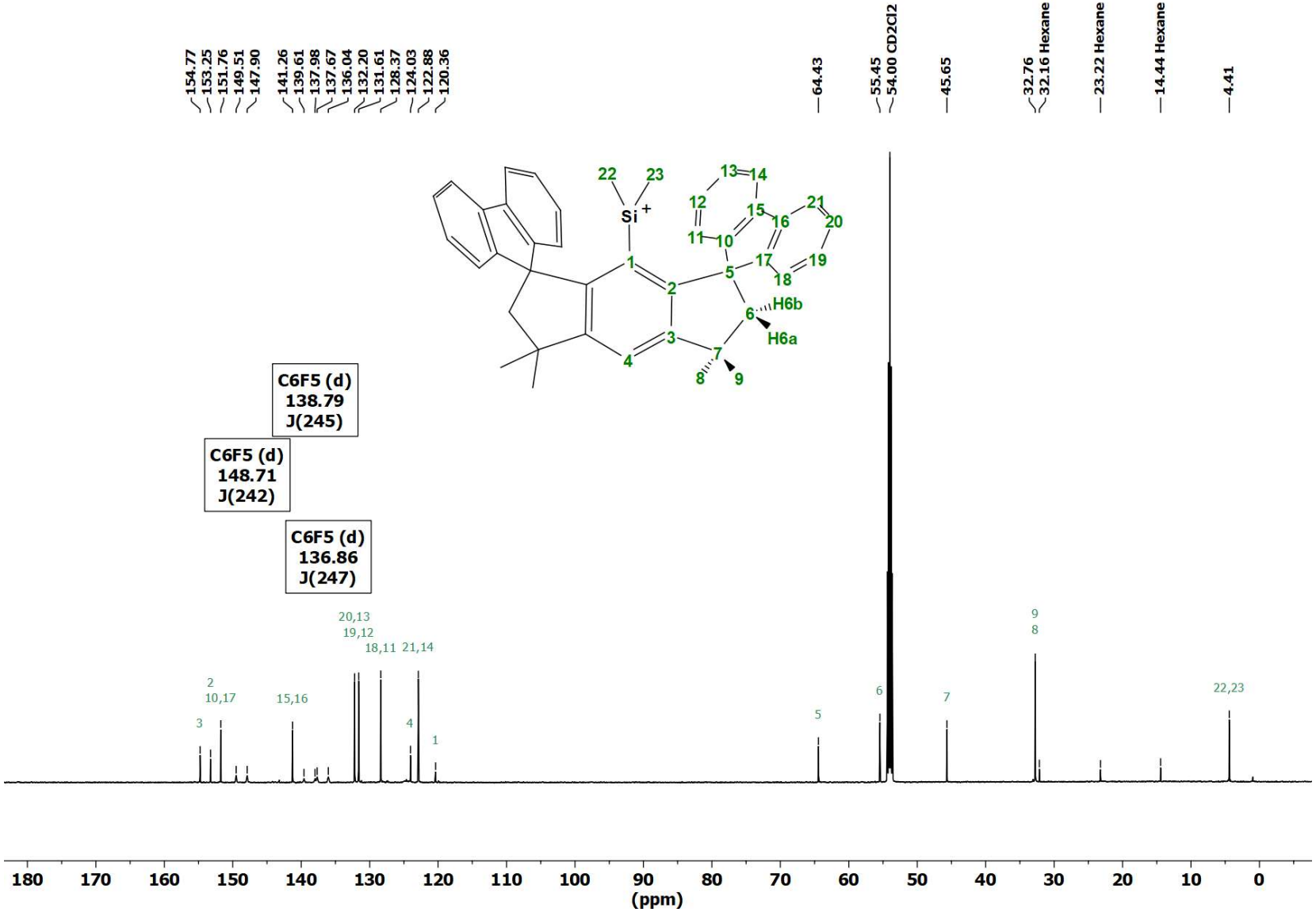

Figure S18. $^{13}C\{^{1}H\}$ NMR (CD_2Cl_2, 151 MHz) spectrum of **1Si**.

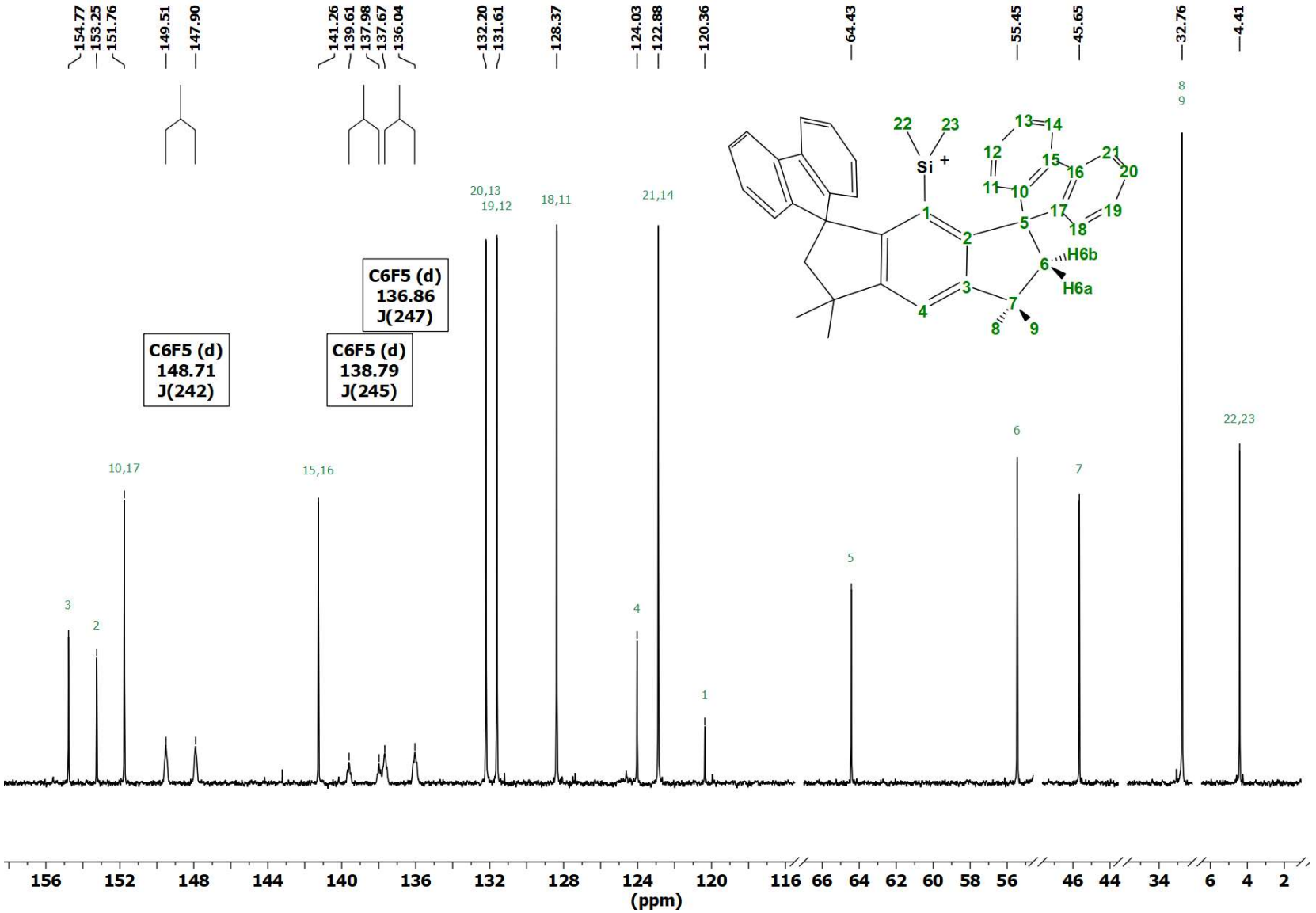

Figure S19. Detailed $^{13}C\{^{1}H\}$ NMR (CD_2Cl_2, 151 MHz) spectrum of **1Si**.

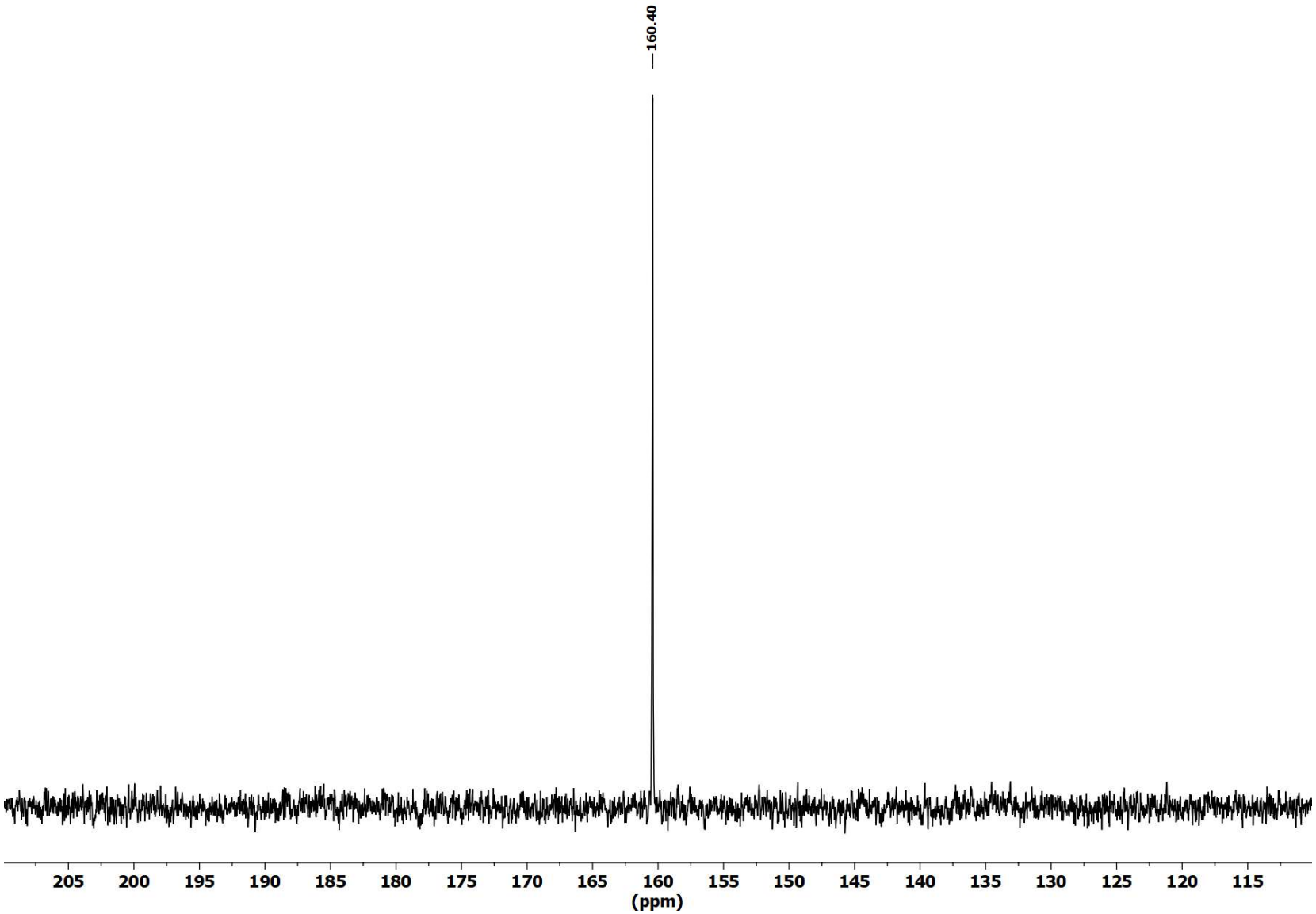

Figure S20. $^{29}Si\{^{1}H\}$ NMR (CD_2Cl_2, 119 MHz) spectrum of **1Si**.

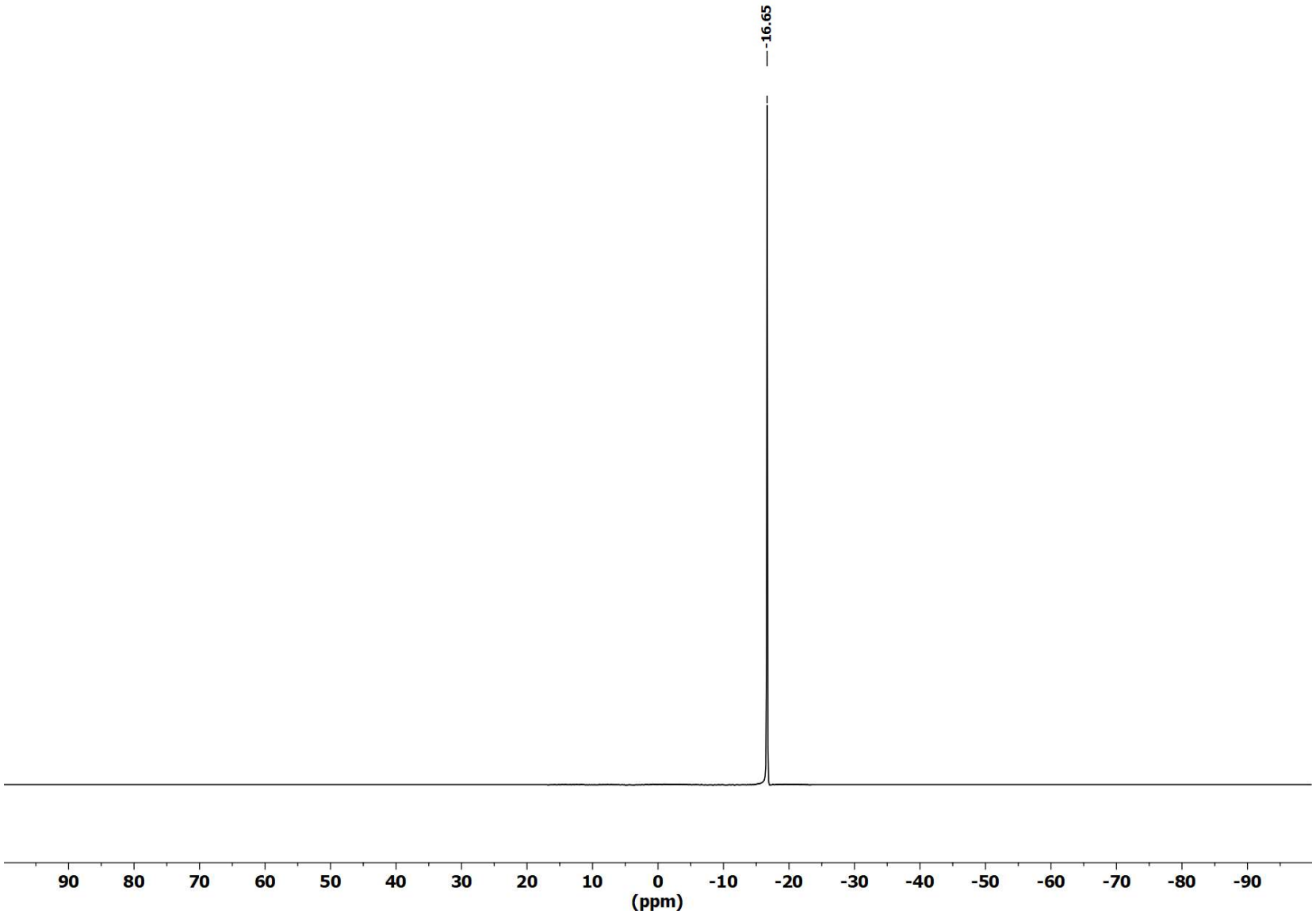

Figure S21. ^{11}B NMR (CD_2Cl_2, 193 MHz) spectrum of **1Si**.

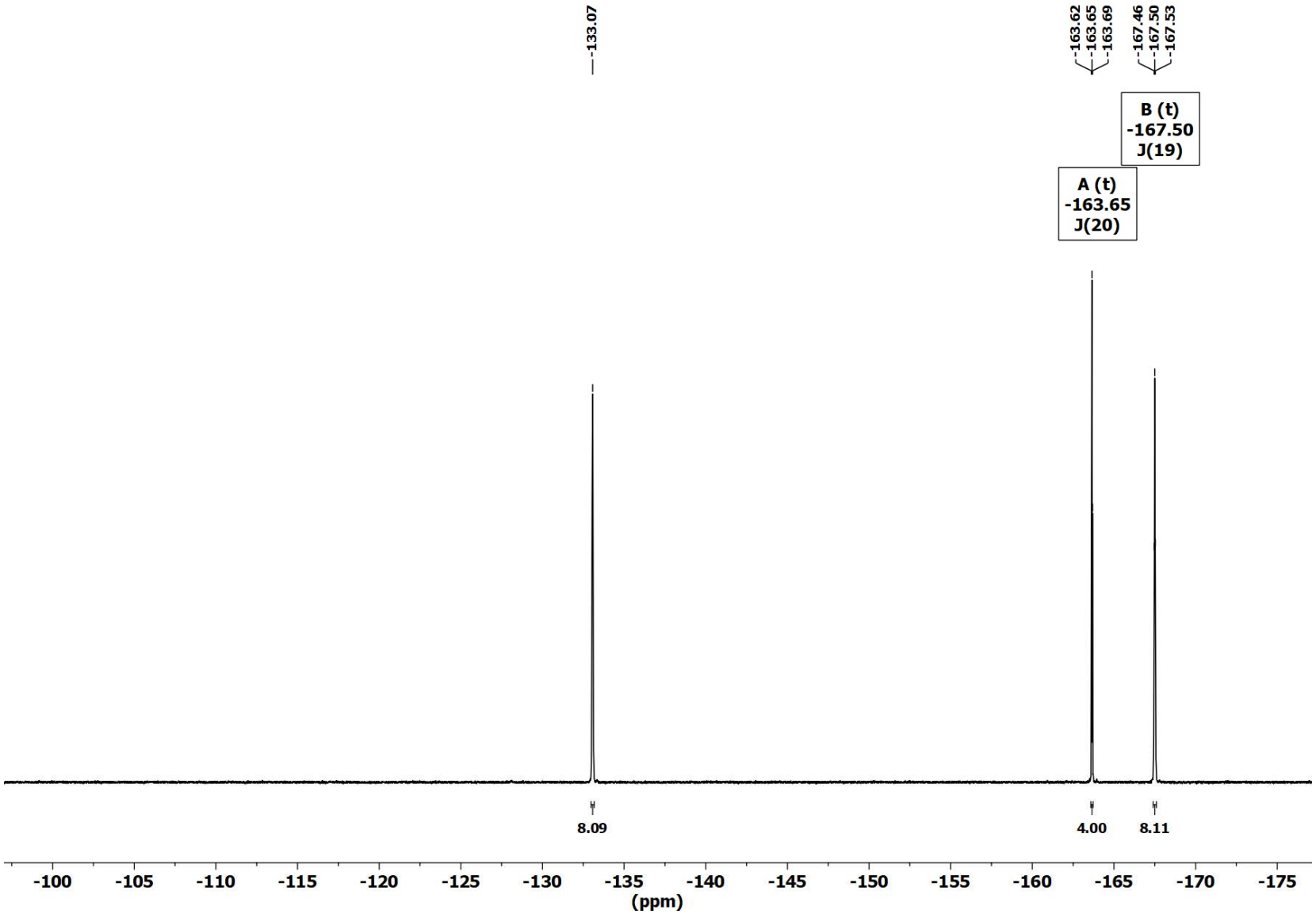

Figure S22. ^{19}F NMR (CD_2Cl_2, 565 MHz) spectrum of **1Si**.

Synthesis and characterization of [$R_{ind}SnMe_2$][$B(C_6F_5)_4$] (1Sn)

To a solid mixture of $R_{ind}SnMe_2Cl$ (**2**) (0.180 g, 0.258 mmol) and $K[B(C_6F_5)_4]$ (0.185 g, 0.258 mmol) was added dichloromethane (8 mL) and the reaction mixture was stirred at room temperature for 1 hour. The reaction mixture was filtered under argon through a PFTE syringe filter to remove KCl. Hexane (16 mL) was layered over the filtrate. The crystalline product was washed with hexane (3 × 5 mL) and dried at reduced pressure. [$R_{ind}SnMe_2$][$B(C_6F_5)_4$] (**1Sn**) was obtained as a colourless solid (0.185 g, 0.138 mmol, 53%).

^{1}H NMR (600 MHz, CD_2Cl_2): δ = 7.62 (dt, $^3J(^1H\text{-}^1H)$ = 8 Hz, $^4J(^1H\text{-}^1H)$ = 1 Hz, 4H, H14, H21), 7.47 (s, $^5J(^1H\text{-}^{119}Sn)$ = 11 Hz, 1H, H4), 7.43 (td, $^3J(^1H\text{-}^1H)$ = 7 Hz, $^4J(^1H\text{-}^1H)$ = 1 Hz, 4H, H13, H20), 7.36 (td, $^3J(^1H\text{-}^1H)$ = 7 Hz, $^4J(^1H\text{-}^1H)$ = 1 Hz, 4H, H12, H19), 7.25 (dt, $^3J(^1H\text{-}^1H)$ = 8 Hz, $^4J(^1H\text{-}^1H)$ = 1 Hz, 4H, H11, H18), 2.58 (s, 4H, H6a, H6b), 1.68 (s, 12H, H8, H9), −0.53 (s, $^2J(^1H\text{-}^{117/119}Sn)$ = 52 Hz, 6H, H22, H23). **^{13}C{^{1}H} NMR (151 MHz, CD_2Cl_2):** δ = 155.00 (s, C3), 154.75 (s, C2), 153.15 (s, C10, C17), 148.71 (d, br, $^1J(^{13}C\text{–}^{19}F)$ = 241 Hz, C_6F_5), 138.81 (d, br, $^1J(^{13}C\text{–}^{19}F)$ = 244 Hz, C_6F_5), 137.71 (s, C15, C16), 136.87 (d, br, $^1J(^{13}C\text{–}^{19}F)$ = 253 Hz, C_6F_5), 132.42 (s, C1), 131.72 (s, C12, C19), 131.13 (s, C13, C20), 127.20 (s, C11, C18), 122.32 (C14, C21), 122.04 (C4), 64.11 (s, C5), 53.77 (s, C6), 45.79 (s, C7), 32.95 (s, C8, C9), 8.79 (s, $^1J(^{13}C\text{–}^{117/119}Sn)$ = 248/259 Hz, C22, C23). **^{119}Sn{^{1}H} NMR (224 MHz, CD_2Cl_2):** δ = 619.89 (s). **^{11}B NMR (193 MHz, CD_2Cl_2):** δ = −16.64 (s). **^{19}F NMR (565 MHz, CD_2Cl_2):** δ = −133.07 (br, 8F, *o*-C_6F_5), −163.67 (t, $^3J(^{19}F\text{-}^{19}F)$ = 20 Hz, 4F, *p*-C_6F_5), −167.50 (t, br, $^3J(^{19}F\text{-}^{19}F)$ = 19 Hz, 8F, *m*-C_6F_5). **HRMS ESI (m/z):** $[M]^+$ calculated for $C_{42}H_{39}Sn$, 663.20771; found 663.20703.

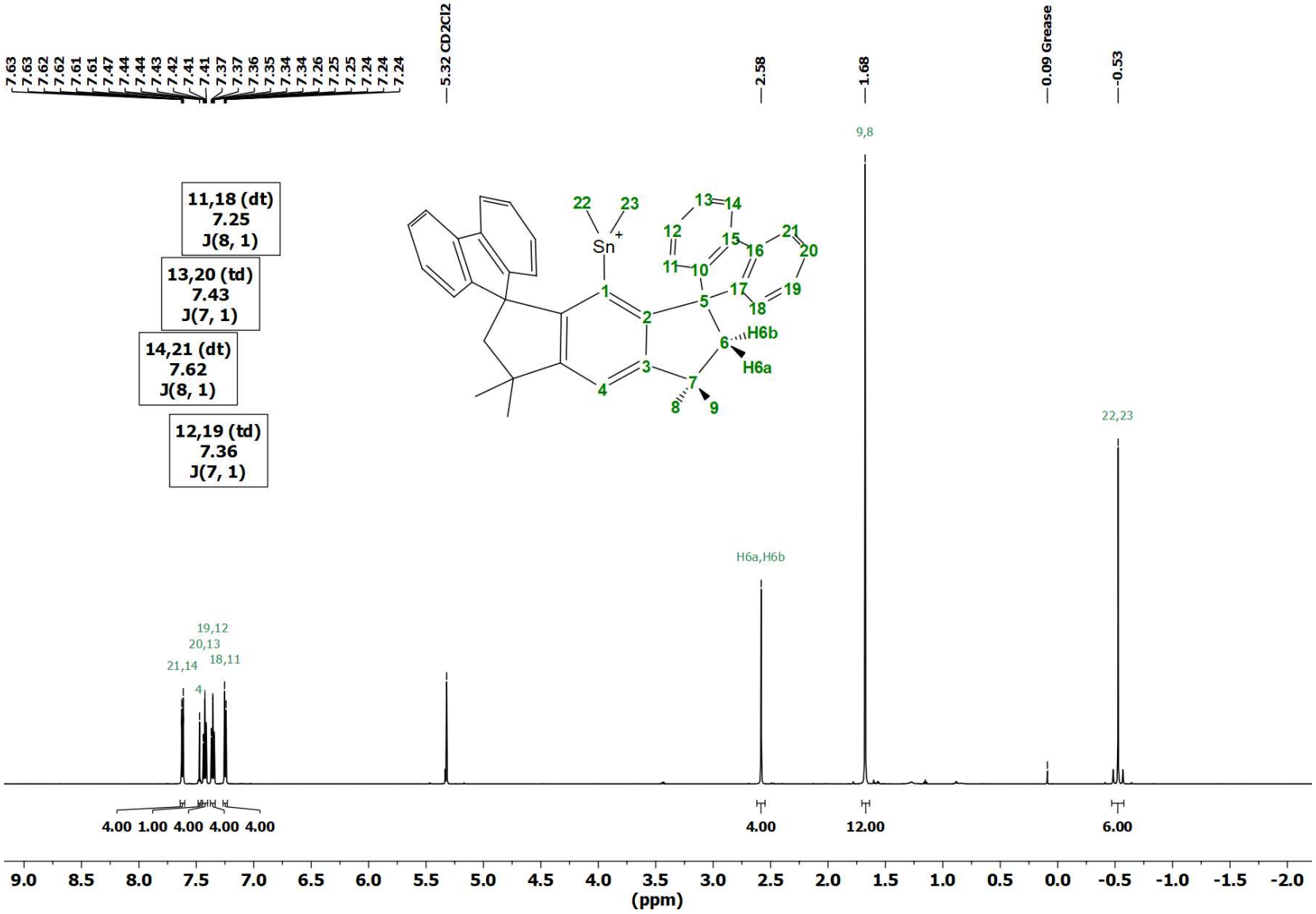

Figure S23. ^{1}H NMR (CD_2Cl_2, 600 MHz) spectrum of **1Sn**.

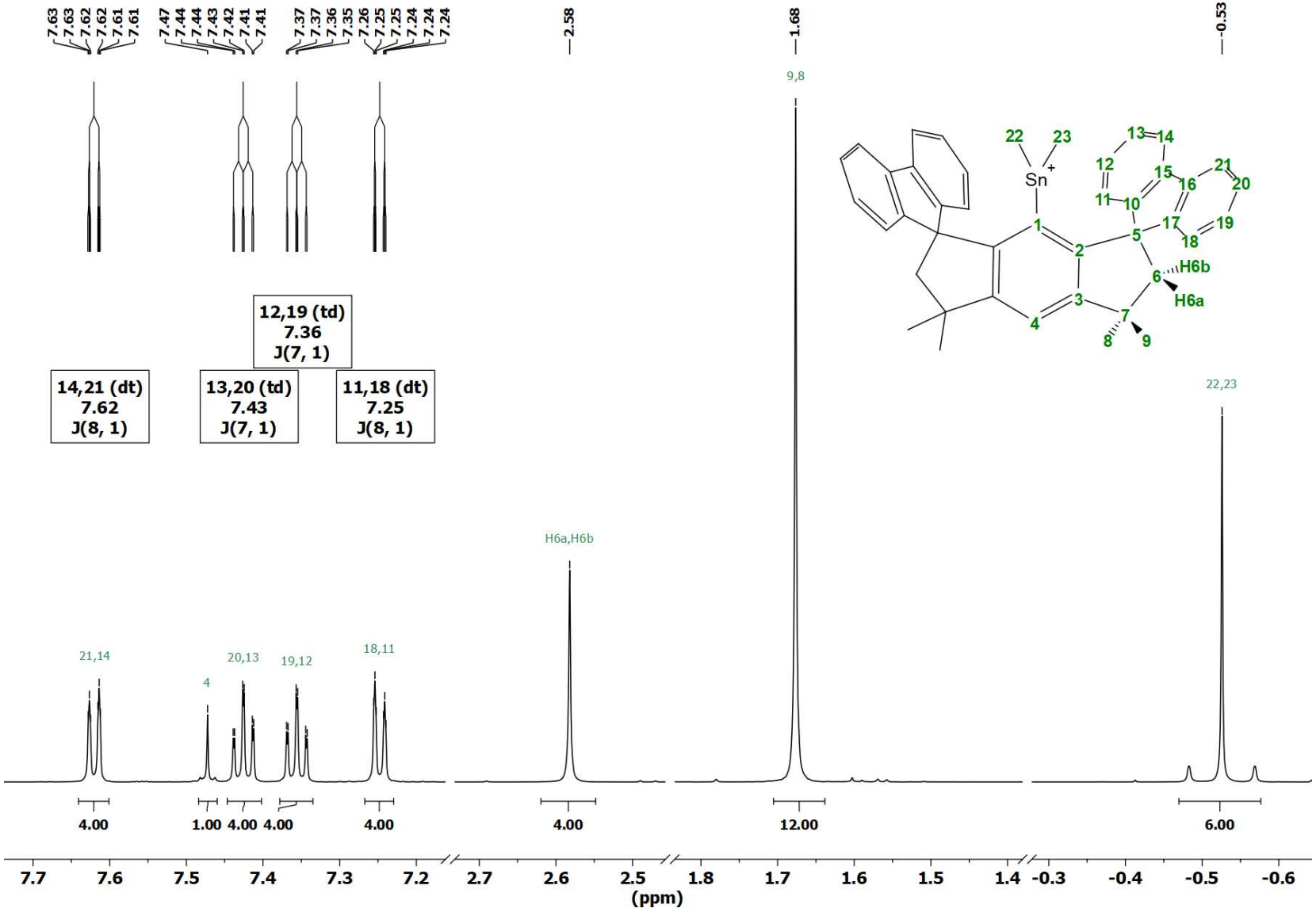

Figure S24. Detailed ^{1}H NMR (CD_2Cl_2, 600 MHz) spectrum of **1Sn**.

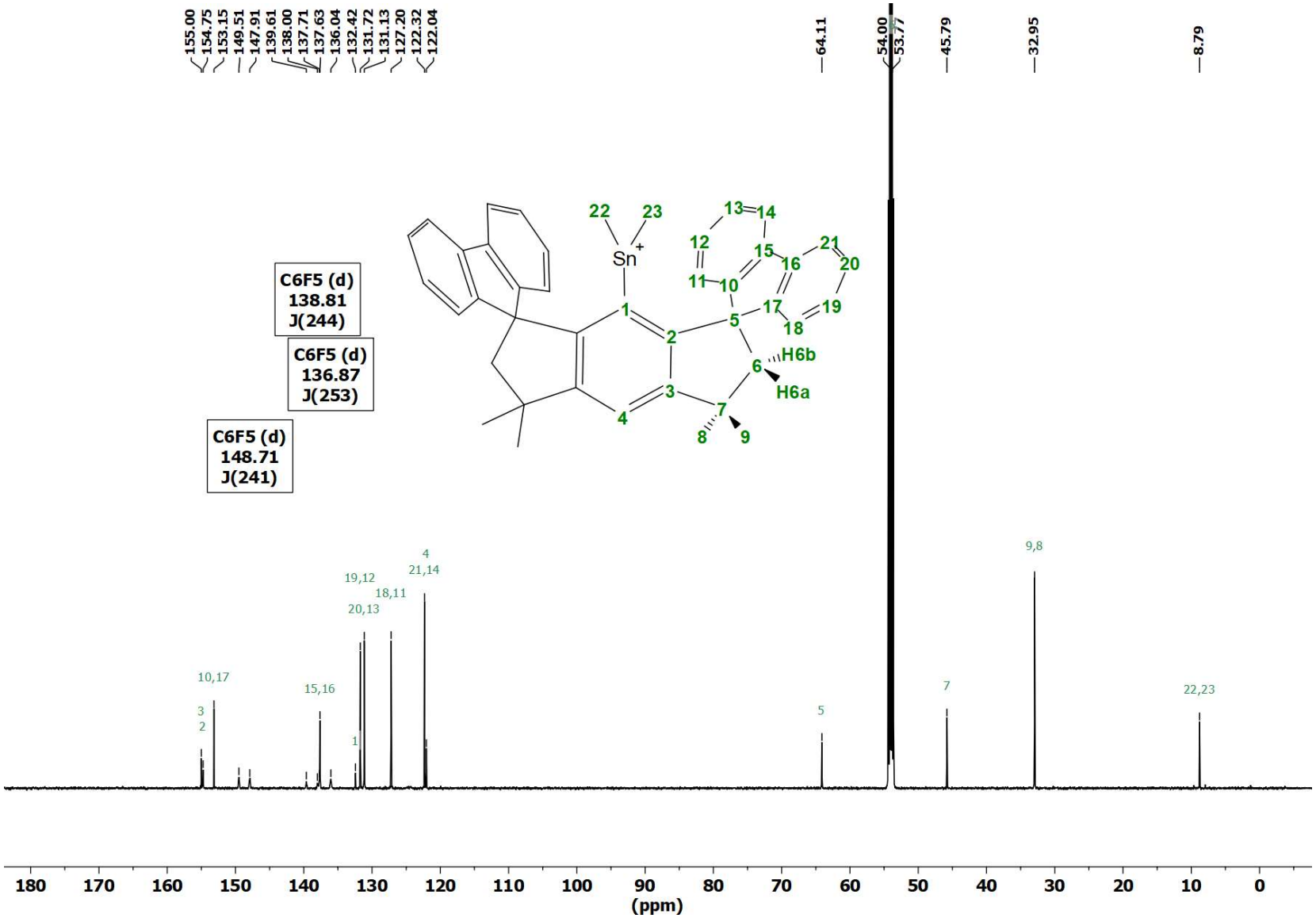

Figure S25. $^{13}C\{^{1}H\}$ NMR (CD_2Cl_2, 151 MHz) spectrum of **1Sn**.

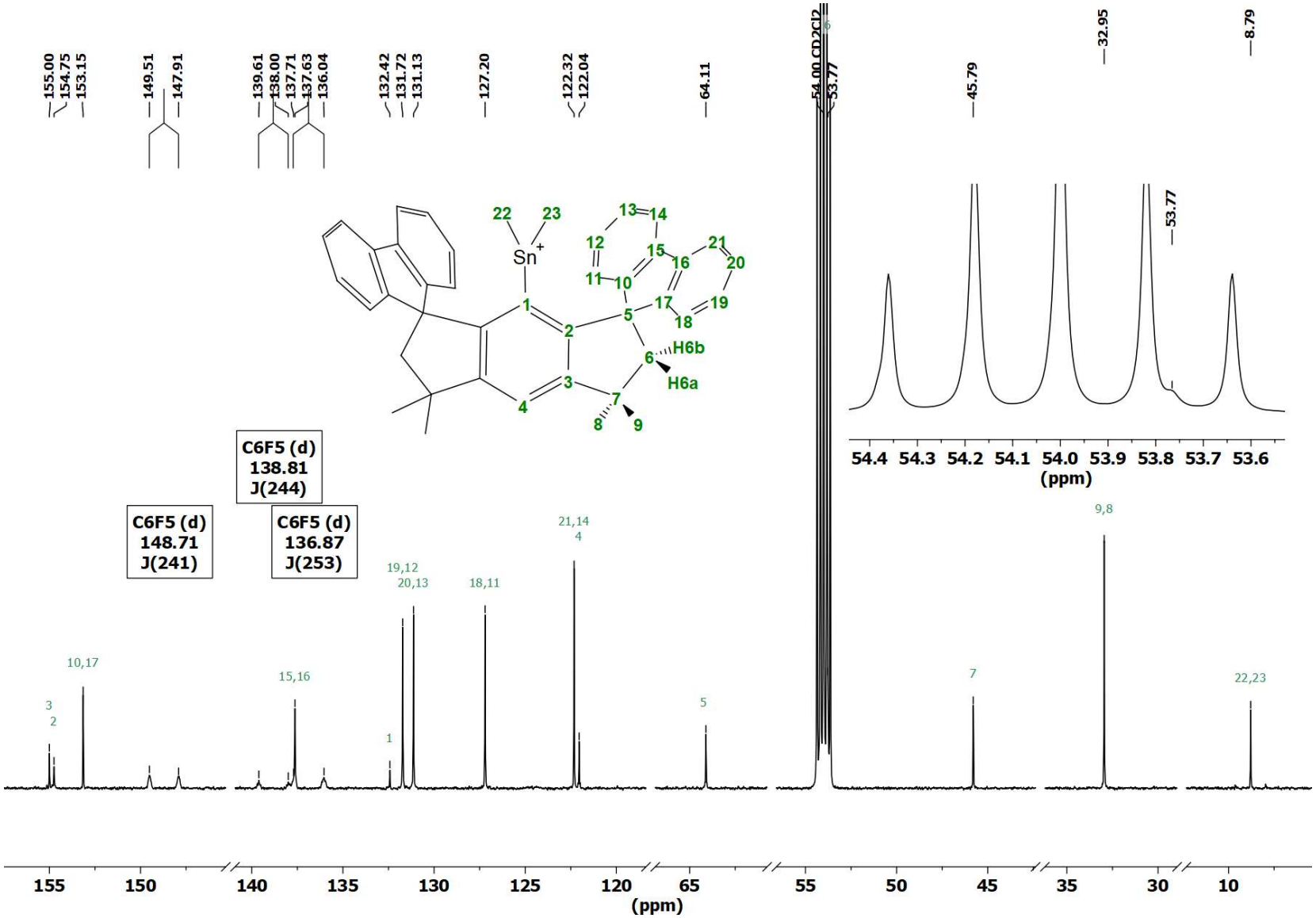

Figure S26. Detailed $^{13}C\{^{1}H\}$ NMR (CD_2Cl_2, 151 MHz) spectrum of **1Sn**.

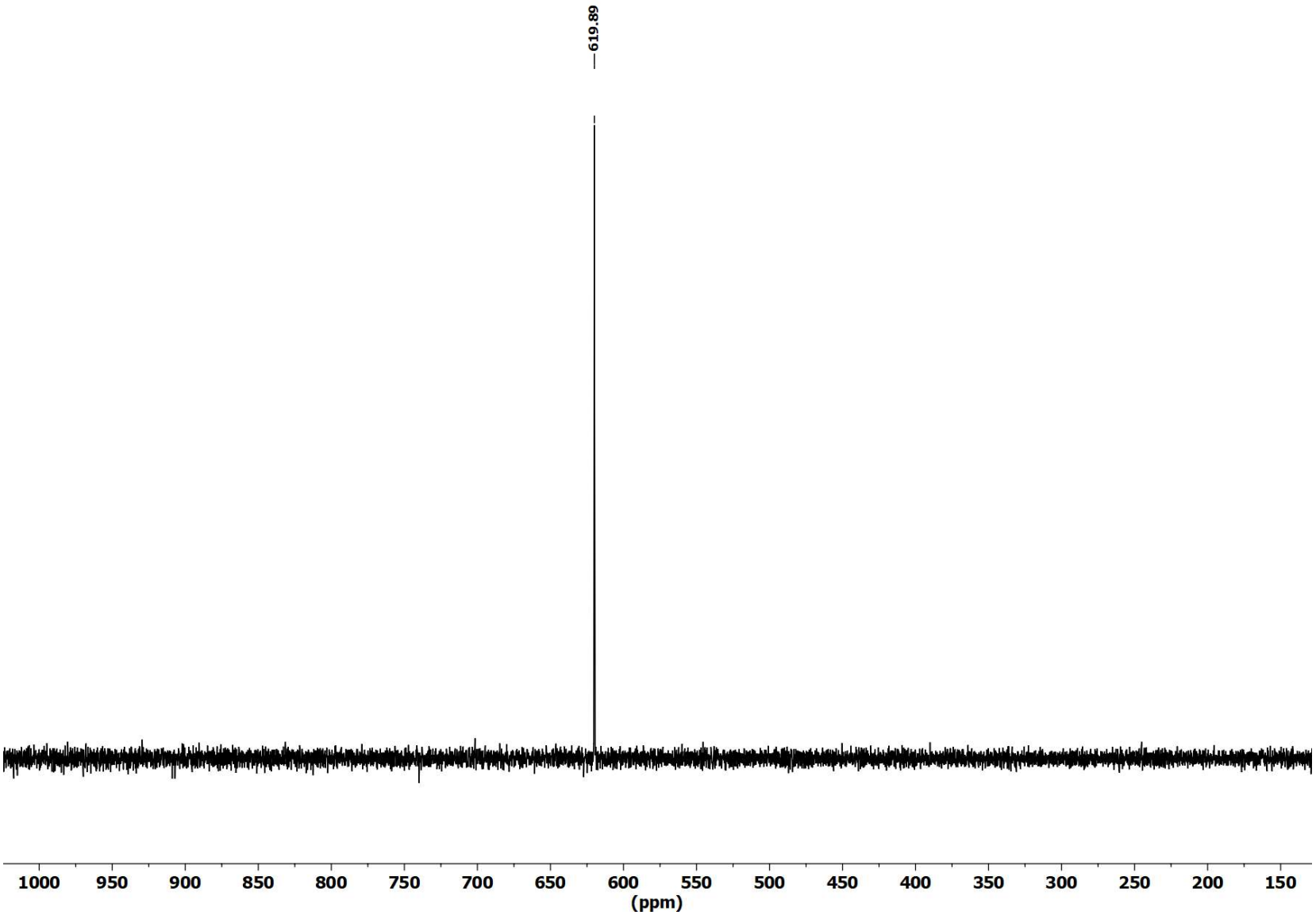

Figure S27. $^{119}Sn\{^{1}H\}$ NMR (CD_2Cl_2, 224 MHz) spectrum of **1Sn**.

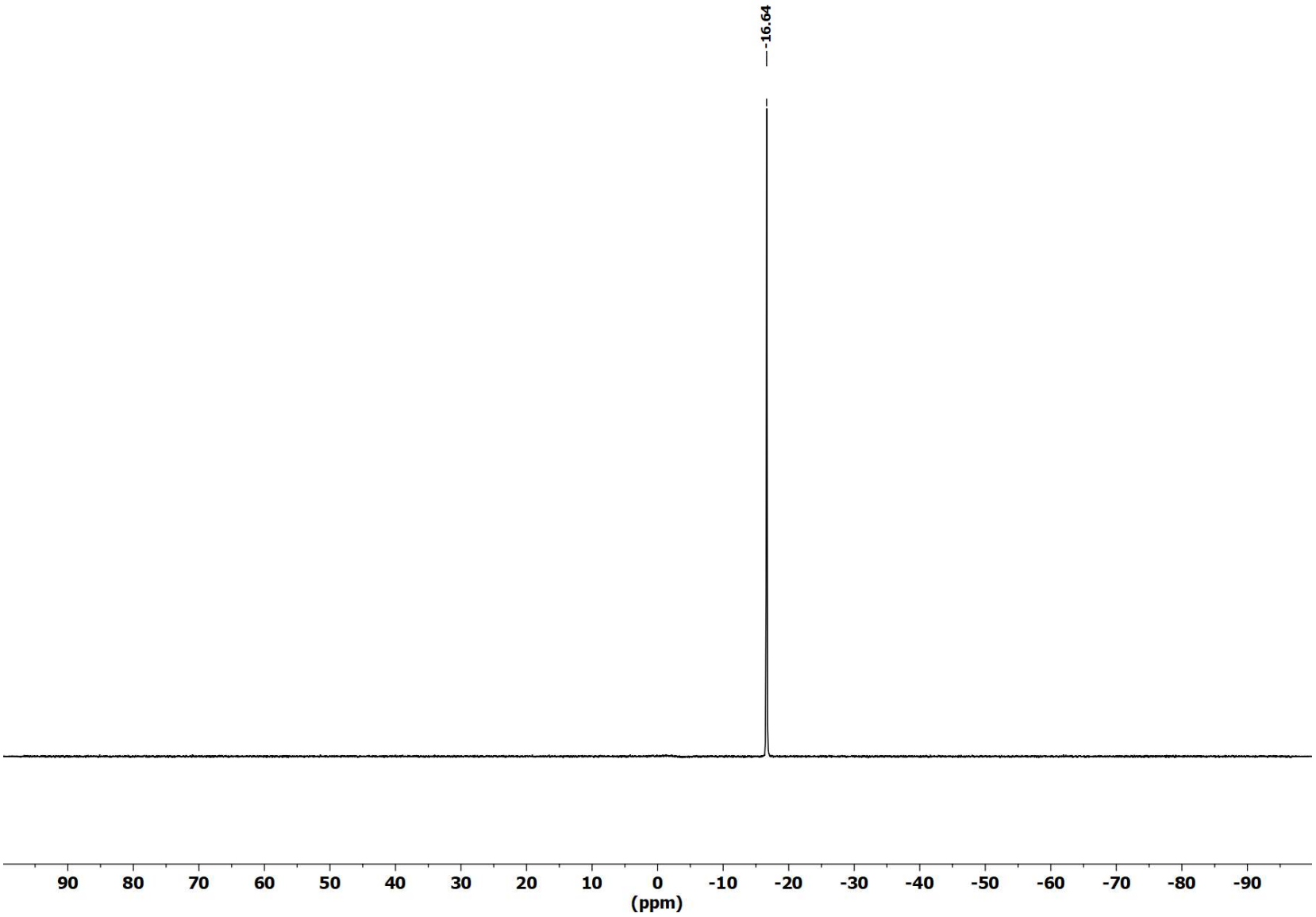

Figure S28. ^{11}B NMR (CD_2Cl_2, 193 MHz) spectrum of **1Sn**.

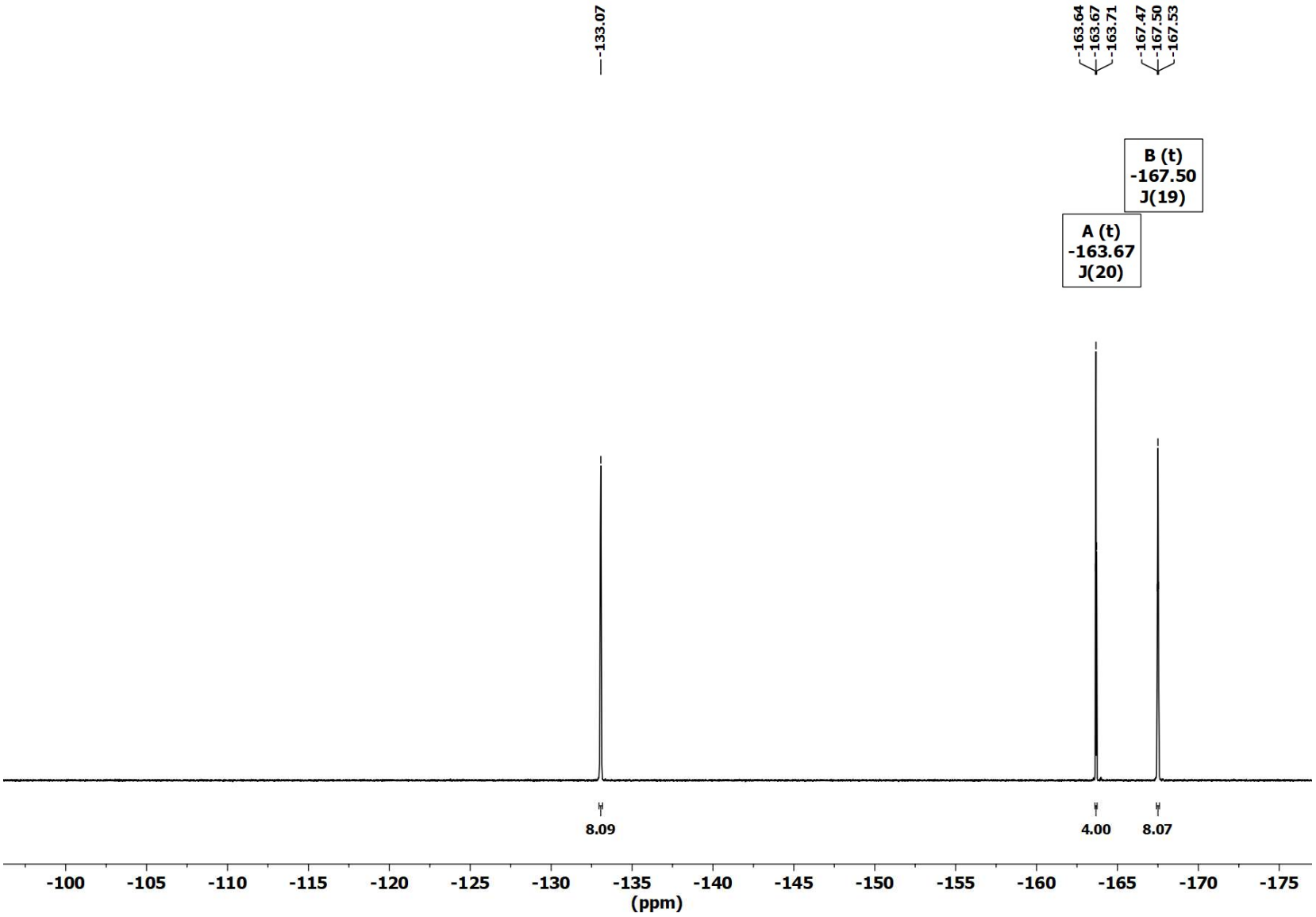

Figure S29. ^{19}F NMR (CD_2Cl_2, 565 MHz) spectrum of **1Sn**.

Synthesis and characterization of [$R_{ind}PbMe_2$][$B(C_6F_5)_4$] (1Pb)

To a solid mixture of $R_{ind}PbMe_3$ (**4**) (184 mg, 0.240 mmol) and $Ph_3C[B(C_6F_5)_4]$ (222 mg, 0.240 mmol) was added dichloromethane (6 mL) and the reaction mixture was stirred at room temperature for 1 hour. The reaction mixture was filtered under argon through a PTFE syringe filter and the filtrate was layered with hexane (18 mL). The resulting crystalline product was washed with hexane (3 × 5 mL) and dried at reduced pressure. [$R_{ind}PbMe_2$][$B(C_6F_5)_4$] (**1Pb**) was obtained as a pale yellow crystalline solid (140 mg, 0.098 mmol, 41%).

^{1}H NMR (600 MHz, CD_2Cl_2): δ = 7.59 (dt, $^3J(^1H\text{-}^1H)$ = 8 Hz, $^4J(^1H\text{-}^1H)$ = 1 Hz, 4H, H14, H21), 7.52 (s, $^5J(^1H\text{-}^{207}Sn)$ = 22 Hz, 1H, H4), 7.38 (td, $^3J(^1H\text{-}^1H)$ = 7 Hz, $^4J(^1H\text{-}^1H)$ = 1 Hz, 4H, H13, H20), 7.33 (td, $^3J(^1H\text{-}^1H)$ = 7 Hz, $^4J(^1H\text{-}^1H)$ = 1 Hz, 4H, H12, H19), 7.24 (dt, $^3J(^1H\text{-}^1H)$ = 8 Hz, $^4J(^1H\text{-}^1H)$ = 1 Hz, 4H, H11, H18), 2.57 (s, 4H, H6a, H6b), 1.68 (s, 12H, H8, H9), 0.34 (s, $^2J(^1H\text{-}^{207}Pb)$ = 55 Hz, 6H, H22, H23). **^{13}C{^{1}H} NMR (151 MHz, CD_2Cl_2):** δ = 161.76 (s, C1), 157.65 (s, $^3J(^{13}C\text{–}^{207}Pb)$ = 56 Hz, C3), 155.96 (s, $^2J(^{13}C\text{–}^{207}Pb)$ = 35 Hz, C2), 153.03 (s, C10,C17), 148.74 (d, br, $^1J(^{13}C\text{-}^{19}F)$ = 242 Hz, C_6F_5), 138.83 (d, br, $^1J(^{13}C\text{–}^{19}F)$ = 243 Hz, C_6F_5), 137.19 (s, C15, C16), 136.89 (d, br, $^1J(^{13}C\text{–}^{19}F)$ = 247 Hz, C_6F_5), 131.31 (s, C12, C19), 130.80 (s, C13, C20), 126.95 (s, C11, C18), 121.71 (C14, C21), 120.59 (C4), 63.65 (s, C5), 53.39 (s, C6), 46.32 (s, C7),35.51 (s, $^1J(^{13}C\text{–}^{207}Pb)$ = 44 Hz, C22,C23), 33.09 (s, C8, C9). **^{207}Pb{^{1}H} NMR (126 MHz, CD_2Cl_2):** 1549.54 (s). **^{11}B NMR (193 MHz, CD_2Cl_2):** δ = −16.64 (s). **^{19}F NMR (565 MHz, CD_2Cl_2):** δ = −133.09 (br, 8F, *o*-C_6F_5), −163.67 (t, $^3J(^{19}F\text{-}^{19}F)$ = 20 Hz, 4F, *p*-C_6F_5), −167.50 (t, br, $^3J(^{19}F\text{-}^{19}F)$ = 19 Hz, 8F, *m*-C_6F_5). **HRMS ESI (m/z):** $[M]^+$ calculated for $C_{42}H_{39}Pb$, 751.28186; found 751.28102.

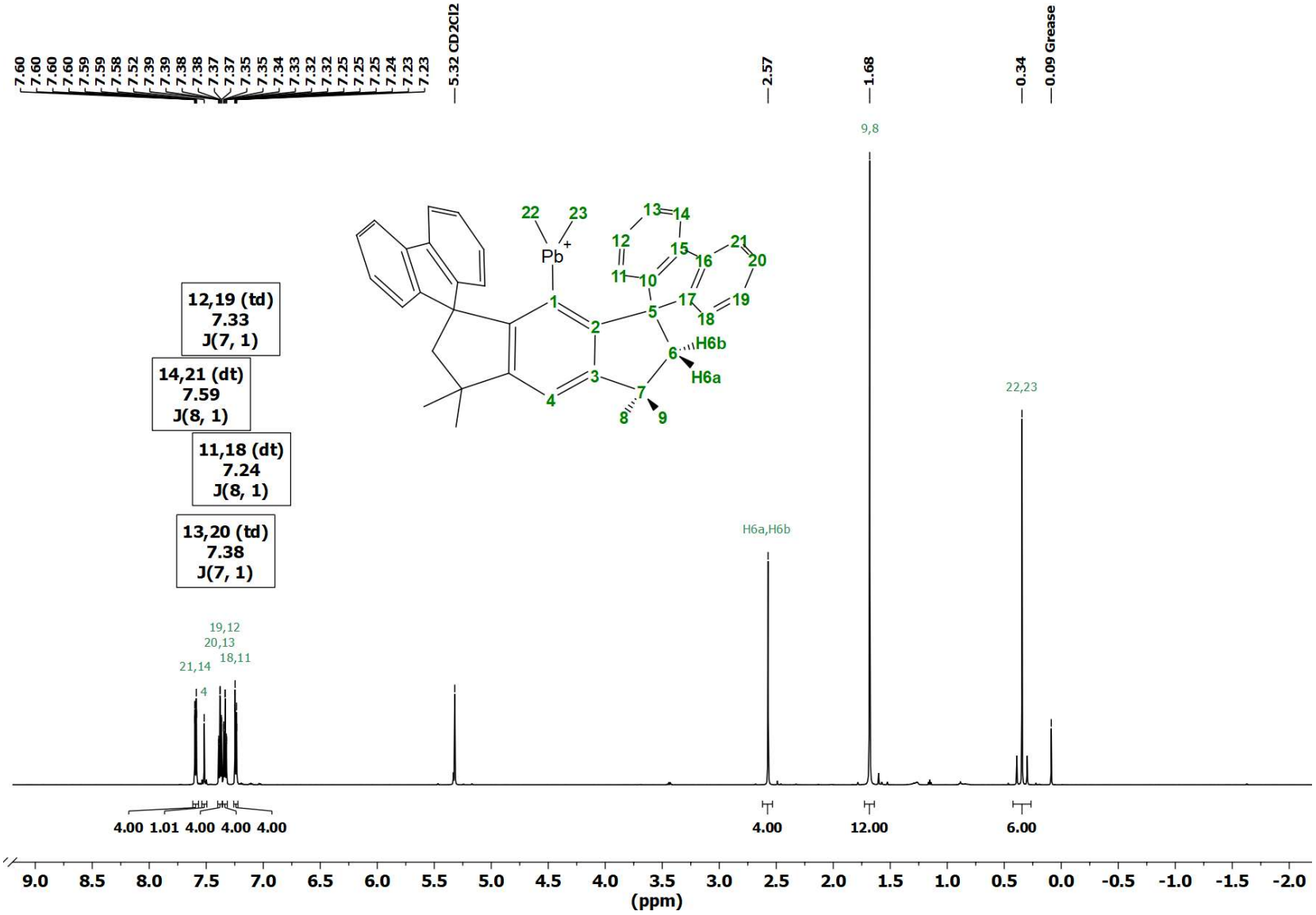

Figure S30. ^{1}H NMR (CD_2Cl_2, 600 MHz) spectrum of **1Pb**.

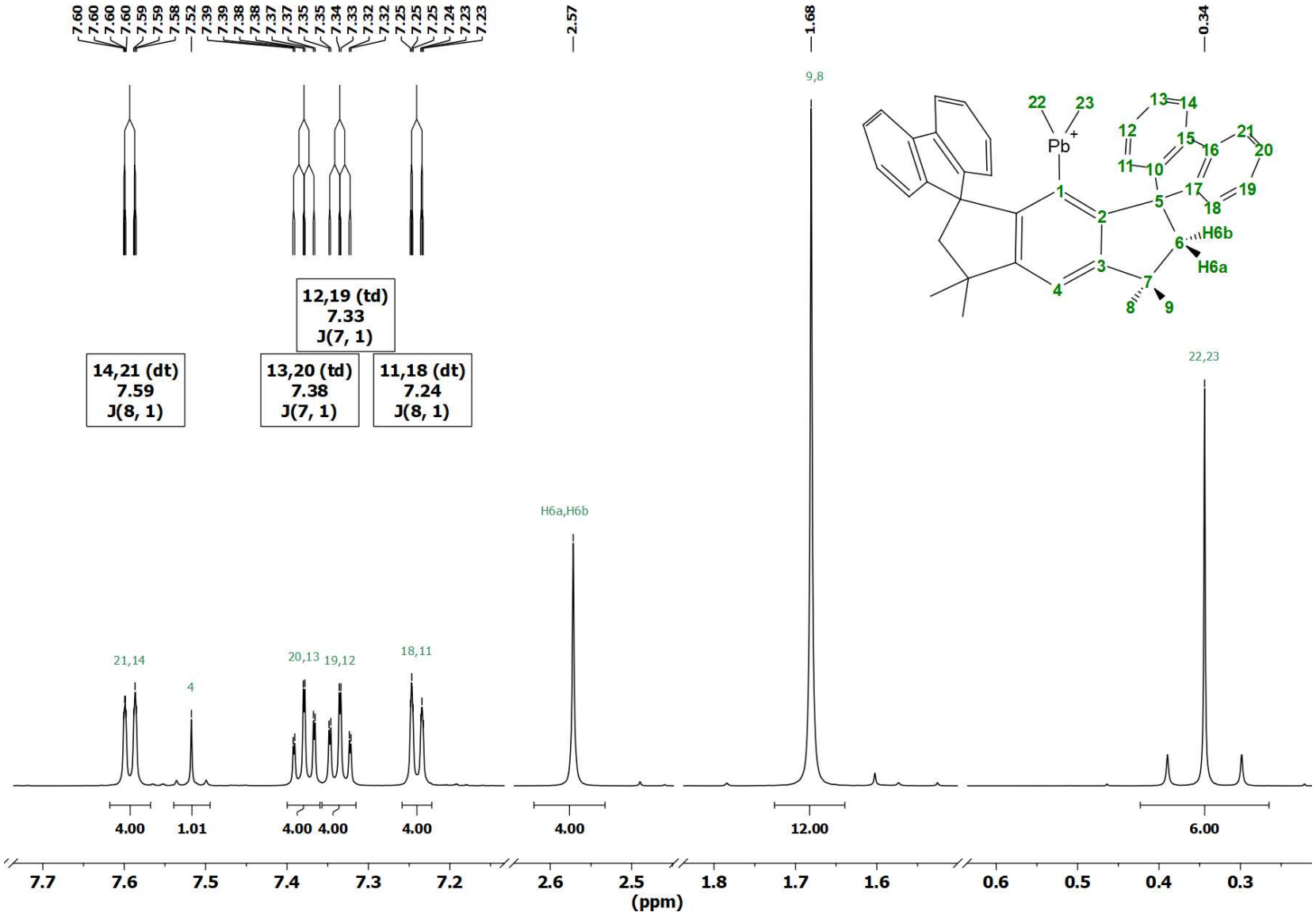

Figure S31. Detailed ^{1}H NMR (CD_2Cl_2, 600 MHz) spectrum of **1Pb**.

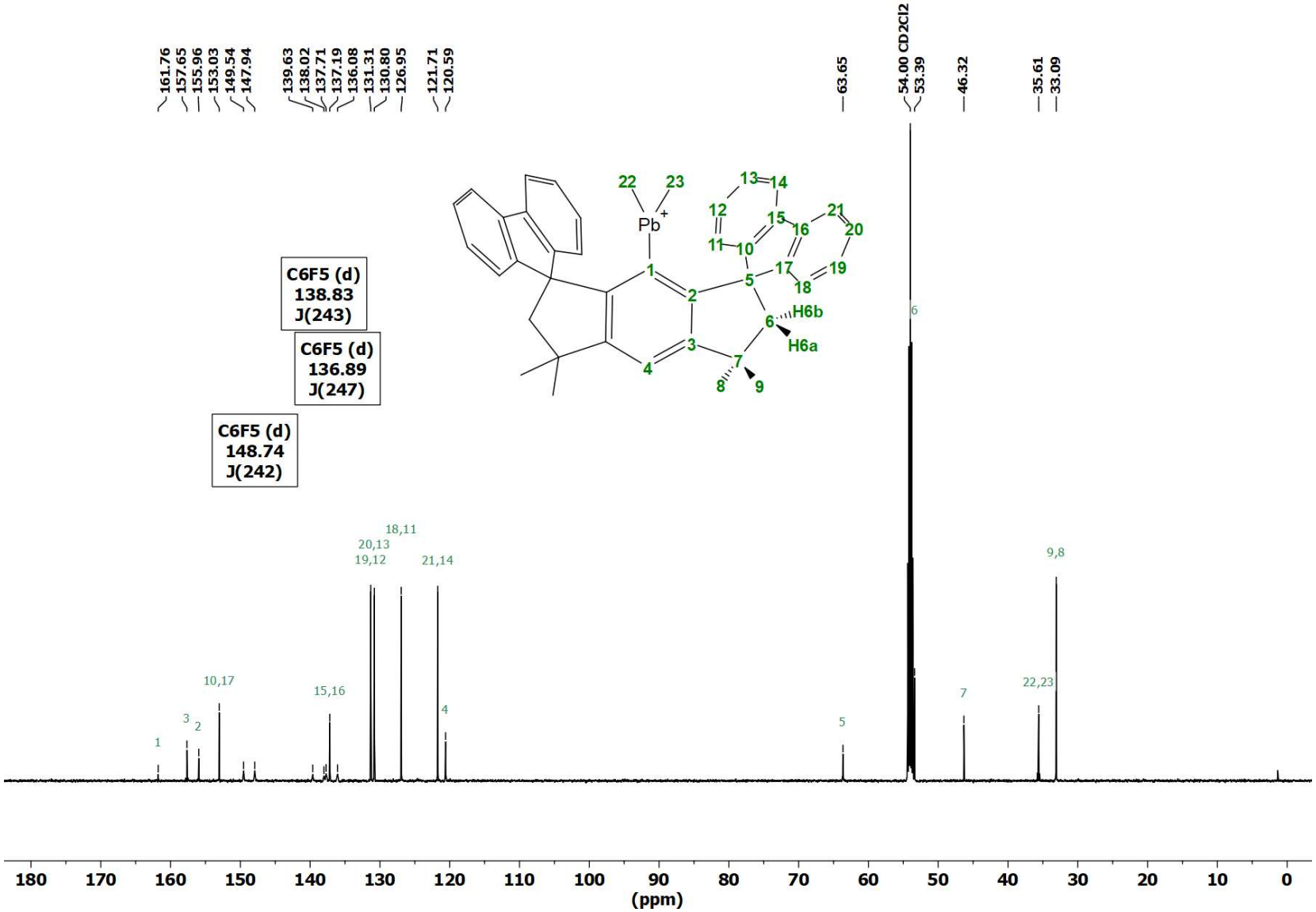

Figure S32. $^{13}C\{^{1}H\}$ NMR (CD_2Cl_2, 151 MHz) spectrum of **1Pb**.

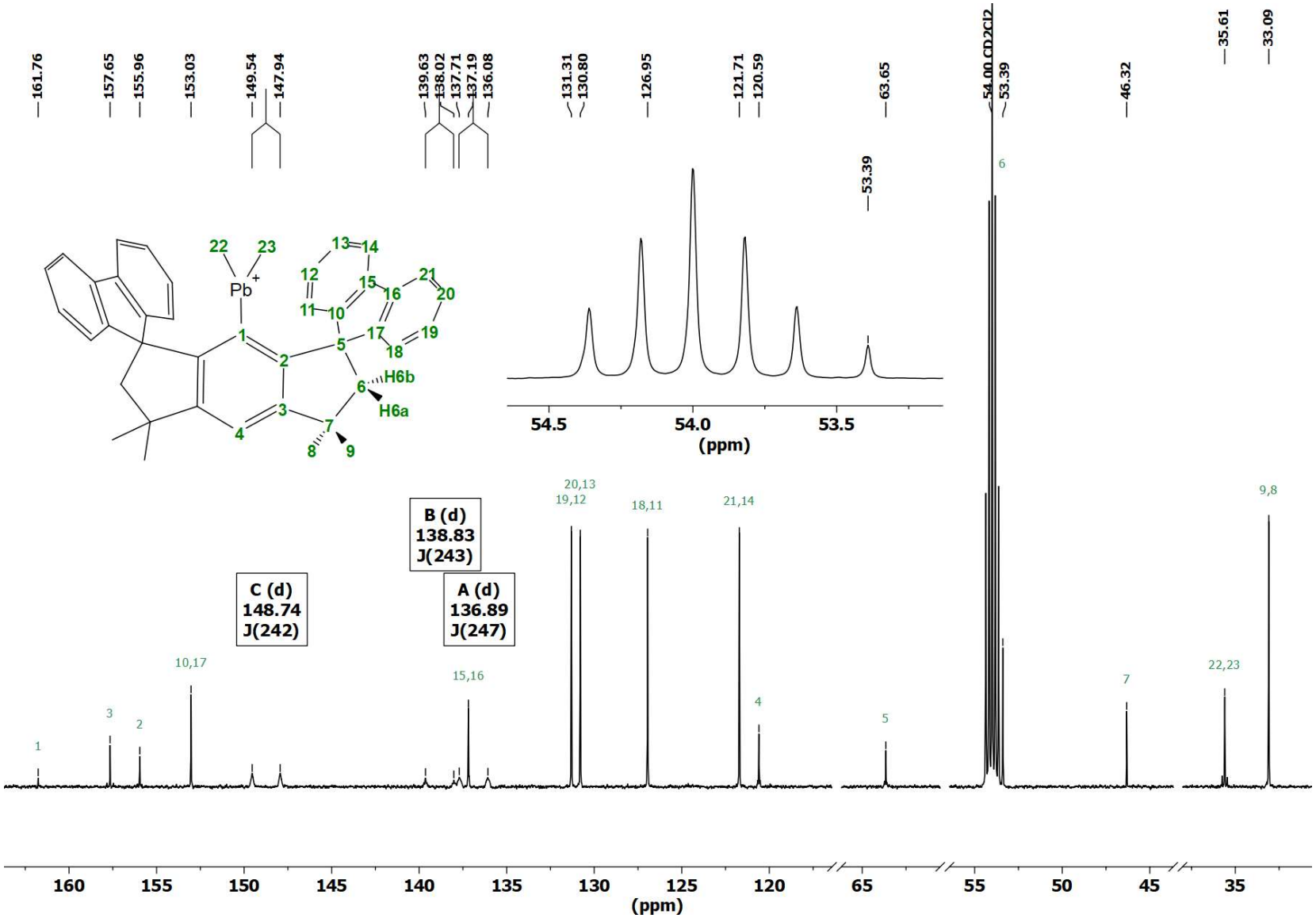

Figure S33. Detailed $^{13}C\{^{1}H\}$ NMR (CD_2Cl_2, 151 MHz) spectrum of **1Pb**.

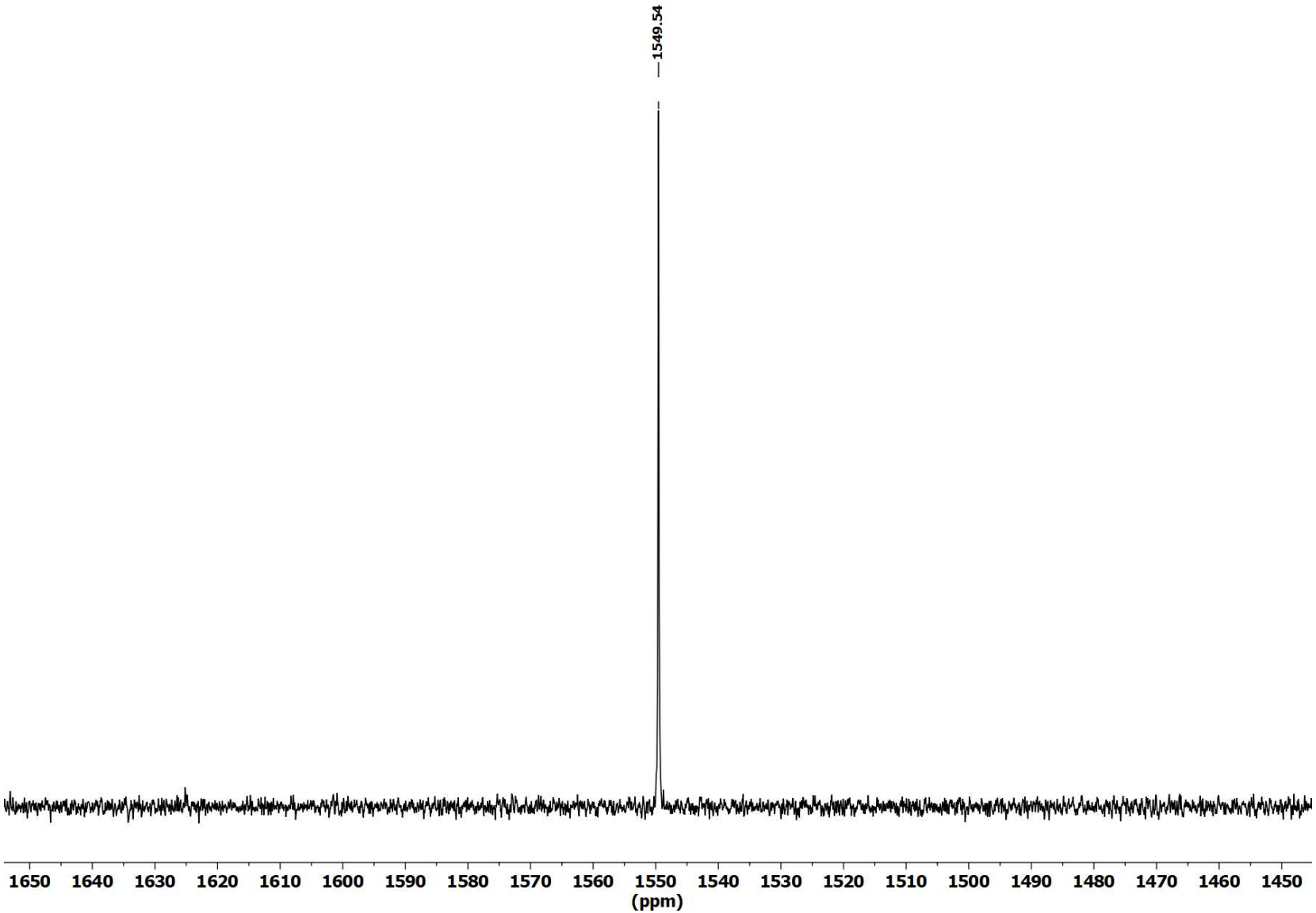

Figure S34. $^{207}Pb\{^{1}H\}$ NMR (CD_2Cl_2, 126 MHz) spectrum of **1Pb**.

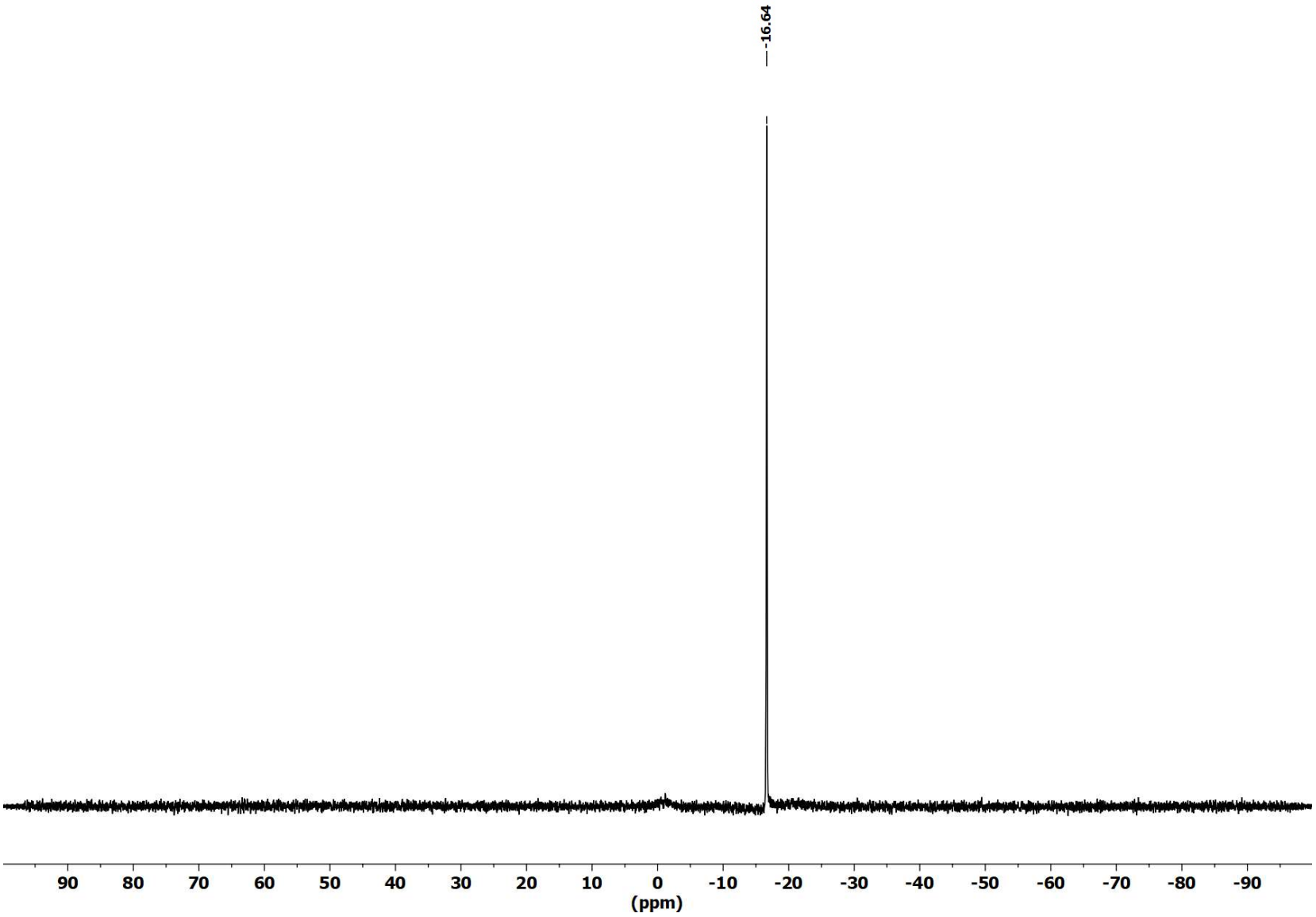

Figure S35. ^{11}B NMR (CD_2Cl_2, 193 MHz) spectrum of **1Pb**.

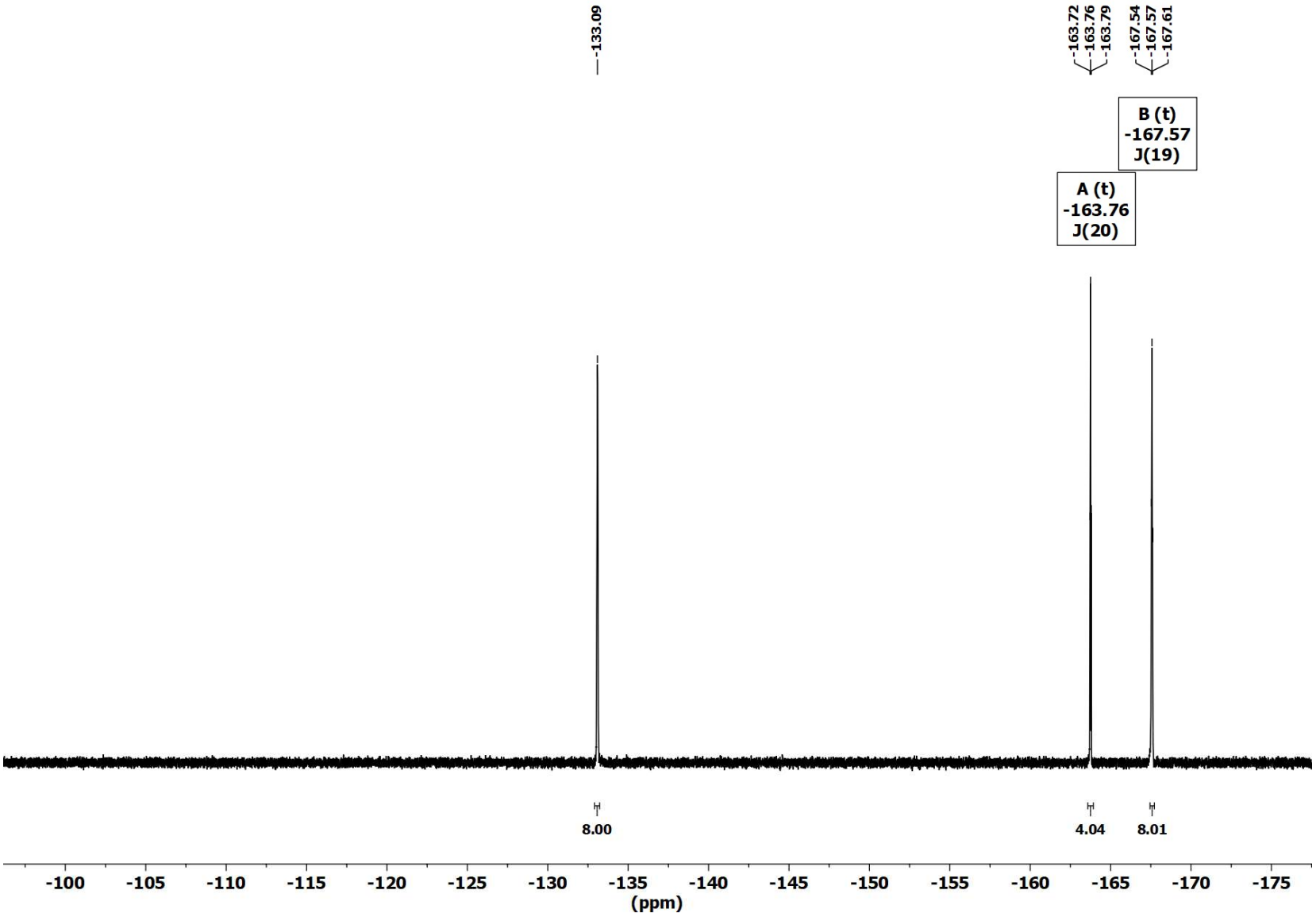

Figure S36. ^{19}F NMR (CD_2Cl_2, 565 MHz) spectrum of **1Pb**.

Determination of Gutmann-Beckett acceptor numbers

Lewis acidity determination experiments by the Gutmann-Beckett method were carried out according to the reported procedure.[S7–S9] A J. Young NMR tube was charged ca. 10-15 mg of the tetrelium salt and an excess of Et_3PO (ca. 3 mg, 2−3 eq) in CD_2Cl_2. The ^{31}P NMR spectra were recorded at room temperature (22 °C) and the chemical shifts are listed in the table below. The acceptor numbers (AN) were determined from the following equation:

$$AN = \frac{\delta_{interacting\ OPEt_3} - 41.0}{86.14 - 41.0} \cdot 100$$

Table S1.

Gutmann-Beckett acceptor numbers

Compound	**^{31}P NMR $OPEt_3$ (ppm)**	**Acceptor Number (AN)**
$[R_{ind}SiMe_2][B(C_6F_5)_4]$ (**1Si**)	89.83	108.2
$[R_{ind}SnMe_2][B(C_6F_5)_4]$ (**1Sn**)	77.93	81.8
$[R_{ind}PbMe_2][B(C_6F_5)_4]$ (**1Pb**)	50.92	21.9

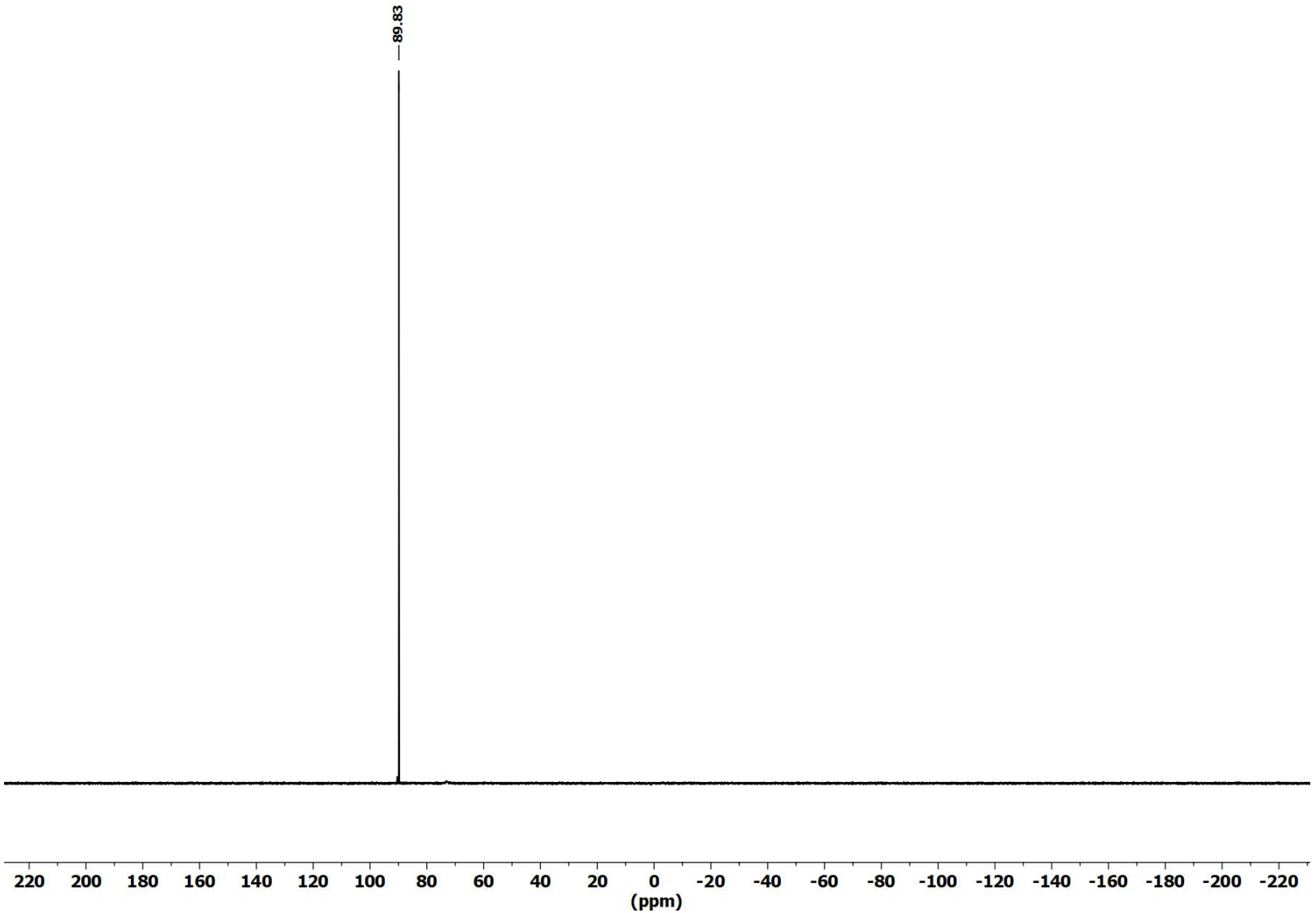

Figure S37. $^{31}P\{^{1}H\}$ NMR (CD_2Cl_2, 243 MHz) spectrum of **1Si** + 2Eq. of Et_3PO.

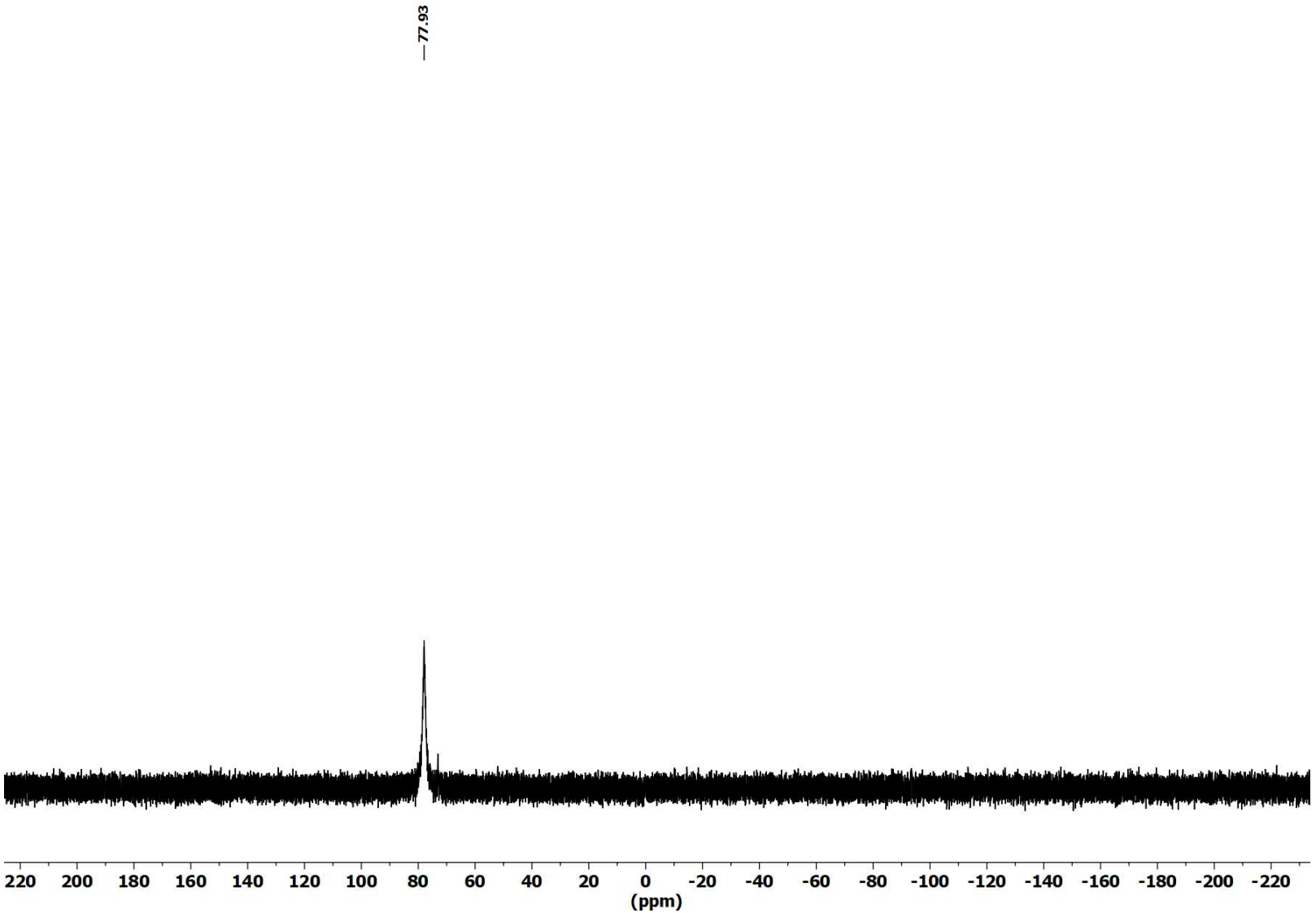

Figure S38. $^{31}P\{^{1}H\}$ NMR (CD_2Cl_2, 243 MHz) spectrum of **1Sn** + 2Eq. of Et_3PO.

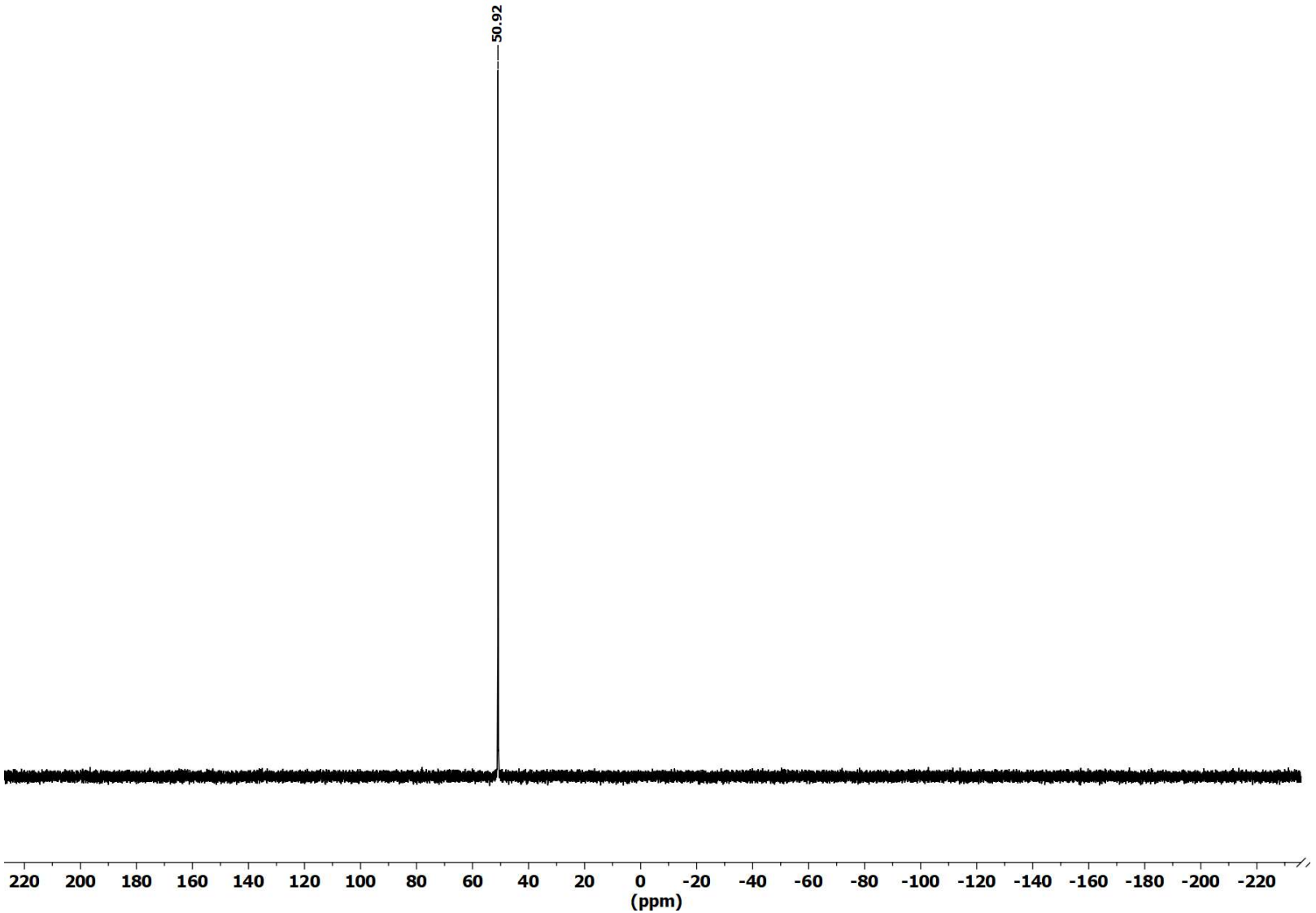

Figure S39. $^{31}P\{^{1}H\}$ NMR (CD_2Cl_2, 243 MHz) spectrum of **1Pb** + 2Eq. of Et_3PO.

Further NMR Experiments

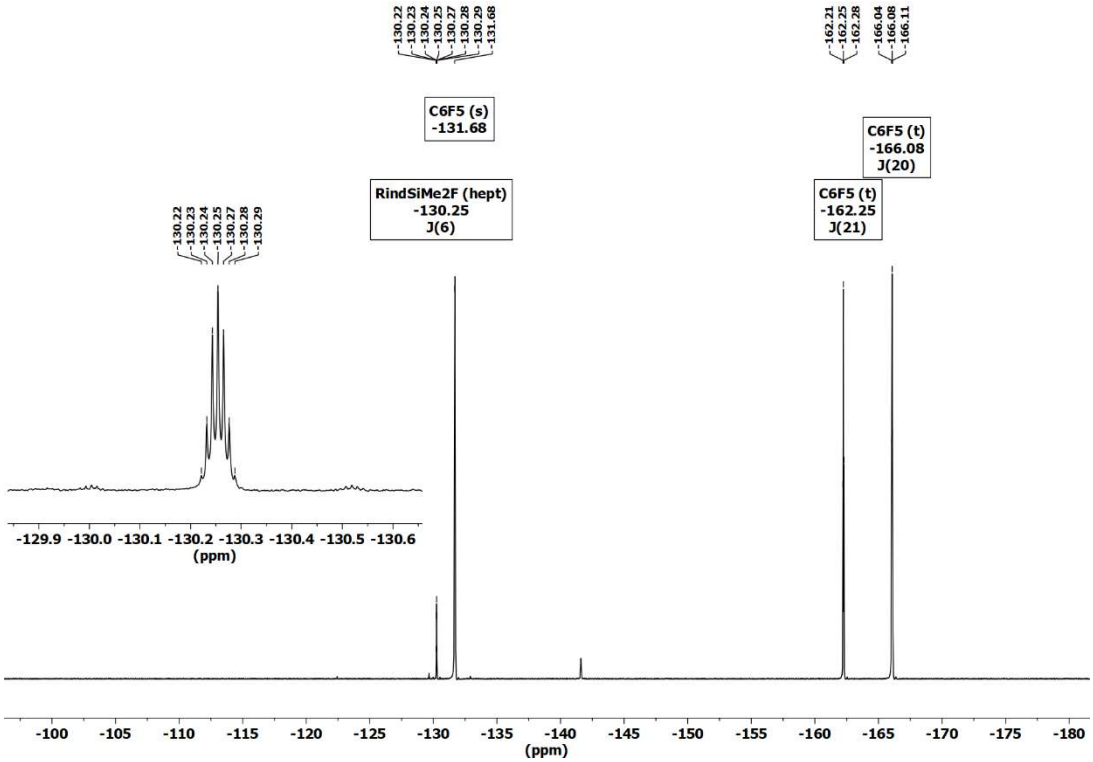

Figure S40. ^{19}F NMR (1,2- $Cl_2C_6D_4$, 565 MHz) spectrum of **1Si** + 1 Eq. of [*n*-Bu_4N][SbF_6].

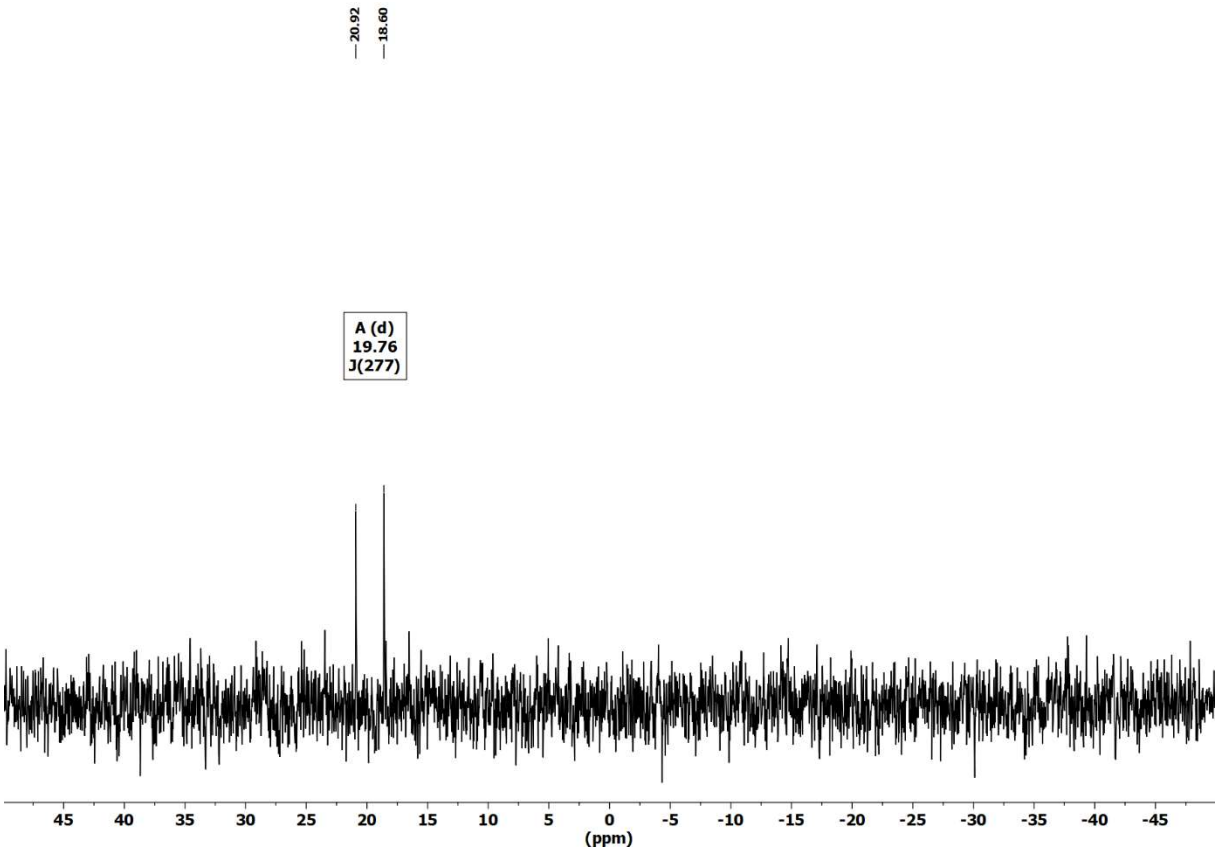

Figure S41. $^{29}Si\{^1H\}$ NMR ($Cl_2C_6D_4$, 119 MHz) spectrum of **1Si** + 1 Eq. of [*n*Bu_4N][SbF_6].

X-Ray Crystallography

Intensity data of **2**, **3**·toluene, **4**, **1Si**, **1Sn** and **1Pb** were collected at 100 K on a Bruker Venture D8 diffractometer with graphite-monochromated Mo-Kα (0.7107 Å) radiation. All structures were solved by direct methods and refined based on F^2 by use of the SHELX program package as implemented in OLEX 1.5.[S10] All non-hydrogen atoms were refined using anisotropic displacement parameters. Hydrogen atoms attached to carbon atoms were included in geometrically calculated positions using a riding model. Disorder was resolved for the methyl groups (and the hydride) of **2** and **3** and refined with split occupancies of 50:50. Diffuse electron density due to disordered solvent molecules of **3** (1/2 toluene), **1Si** (1/2 pentane) and **2Sn** (CH_2Cl_2) was accounted for using the SQUEZZE routine in OLEX. Crystal and refinement data are collected in Table S2 and S3. Figures were created using DIAMOND.[S11] Crystallographic data (excluding structure factors) for the structural analyses have been deposited with the Cambridge Crystallographic Data Centre. Copies of this information may be obtained free of charge from The Director, CCDC, 12 Union Road, Cambridge CB2 1EZ, UK (Fax: +44-1223-336033; e-mail: deposit@ccdc.cam.ac.uk or http://www.ccdc.cam.ac.

Table S2. Crystal data and structure refinement of **2** - **4**.

	2	**3**·toluene	**4**
Formula	$C_{42}H_{40}Si$	$C_{49}H_{47}ClSn$	$C_{43}H_{42}Pb$
Formula weight, g mol^{-1}	572.83	790.00	765.95
Crystal system	triclinic	triclinic	triclinic
Crystal size, mm	0.10 × 0.10 × 0.10	0.20 × 0.20 × 0.15	0.90 × 0.40 × 0.35
Space group	$P\bar{1}$	$P\bar{1}$	$P\bar{1}$
a, Å	9.5487(5)	9.4150(6)	10.1370(7)
b, Å	11.5708(7)	13.8081(8)	12.5545(9)
c, Å	15.9662(11)	15.8413(10)	15.8115(11)
α, º	70.660(3)	82.746(2)	101.750(3)
β, º	80.850(2)	81.826(2)	96.006(3)
γ, º	74.740(2)	70.414(2)	109.536(3)
V, Å^3	1600.80(17)	1913.7(2)	1823.8(2)
Z	2	2	2
ρ_{calcd}, Mg m^{-3}	1.191	1.371	1.395
μ (Mo $K\alpha$), mm^{-1}	0.102	0.771	4.652
F(000)	614	816	764
θ range, deg	2.43 to 25.71	2.34 to 33.22	2.49 to 36.47
Index ranges	–14 ≤ h ≤ 14	– 14 ≤ h ≤ 14	–16 ≤ h ≤ 16
	–17 ≤ k ≤ 17	–21 ≤ k ≤ 21	–20 ≤ k ≤ 20
	–24 ≤ l ≤ 23	–24 ≤ l ≤ 24	–26 ≤ l ≤ 26
No. of reflns collected	70612	70341	72038
Completeness to θ_{max}	99.9%	99.9%	99.8%
No. indep. Reflns	12194	14692	17740
No. obsd reflns with ($I>2\sigma(I)$)	9222	12033	16293
No. refined params	436	816	405
GooF (F^2)	1.068	1.036	1.044
R_1 (F) ($I > 2\sigma(I)$)	0.0547	0.0285	0.0244
wR_2 (F^2) (all data)	0.1543	0.0668	0.0603
Largest diff peak/hole, e Å^{-3}	0.632 / –0.516	0.538 / –0.458	1.928 / –1.305
CCDC number	2227198	2227199	2227200

Table S3. Crystal data and structure refinement of **1Si**, **1Sn** and **1Pb**.

	1Si	**1Sn**	**1Pb**
Formula	$C_{66}H_{39}BF_{20}Si$	$C_{66}H_{39}BF_{20}Sn$	$C_{66}H_{39}BF_{20}Pb$
Formula weight, g mol^{-1}	1250.87	1341.47	1429.97
Crystal system	monoclinic	triclinic	triclinic
Crystal size, mm	0.30 × 0.25 × 0.25	0.15 × 0.15 × 0.10	0.10 × 0.10 × 0.05
Space group	$P2_1/n$	$P\bar{1}$	$P\bar{1}$
a, Å	10.5128(11)	12.6763(9)	10.2803(10)
b, Å	17.7699(16)	12.9768(10)	14.774(2)
c, Å	29.707(3)	17.9122(16)	18.3384(19)
α, º	90	86.226(3)	86.552(7)
β, º	94.346(3)	84.228(3)	78.805(4)
γ, º	90	84.387(3)	85.707(5)
V, Å^3	5533.6(9)	2912.9(4)	2721.6(6)
Z	4	2	2
ρ_{calcd}, Mg m^{-3}	1.501	1.529	1.745
μ (Mo $K\alpha$), mm^{-1}	0.154	0.544	3.213
F(000)	2536	1340	1404
θ range, deg	2.01 to 28.28	1.89 to 30.60	2.02 to 31.59
Index ranges	–14 ≤ h ≤ 14	– 18 ≤ h ≤ 18	–12 ≤ h ≤ 15
	–23 ≤ k ≤ 23	–18 ≤ k ≤ 18	–21 ≤ k ≤ 21
	–39 ≤ l ≤ 39	–25 ≤ l ≤ 25	–26 ≤ l ≤ 26
No. of reflns collected	138018	96017	99714
Completeness to θ_{max}	99.9%	99.9%	99.9%
No. indep. Reflns	13729	17880	16341
No. obsd reflns with ($I>2\sigma(I)$)	9772	15499	18178
No. refined params	799	799	799
GooF (F^2)	1.019	1.056	1.042
R_1 (F) ($I > 2\sigma(I)$)	0.0521	0.0384	0.0256
wR_2 (F^2) (all data)	0.1200	0.0812	0.0525
Largest diff peak/hole, e Å^{-3}	0.535 / –0.432	0.481 / –0.661	0.687 / –0.656
CCDC number	2227201	2227202	2227203

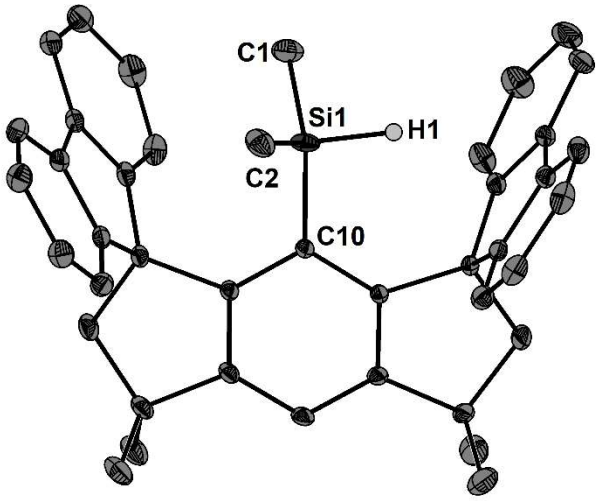

Figure S42. Molecular structure of **2** showing 50% probability ellipsoids and the essential numbering scheme. Selected bond lengths [Å]: Si1-C1 1.807(3), Si1-C2 1.846(3), Si1-C10 1.905(1), Si1-H1 1.47(3).

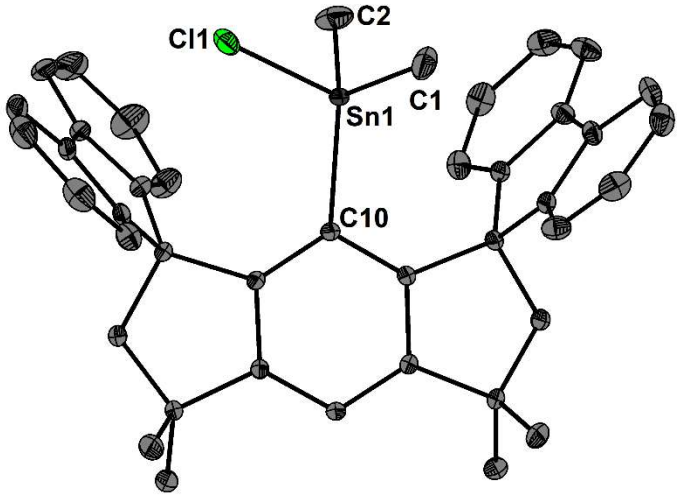

Figure S43. Molecular structure of **3** showing 50% probability ellipsoids and the essential numbering scheme. Selected bond lengths [Å]: Sn1-C1 2.133(3), Sn1-C2 2.115(3), Sn1-C10 2.187(1), Sn1-Cl1 2.342(1).

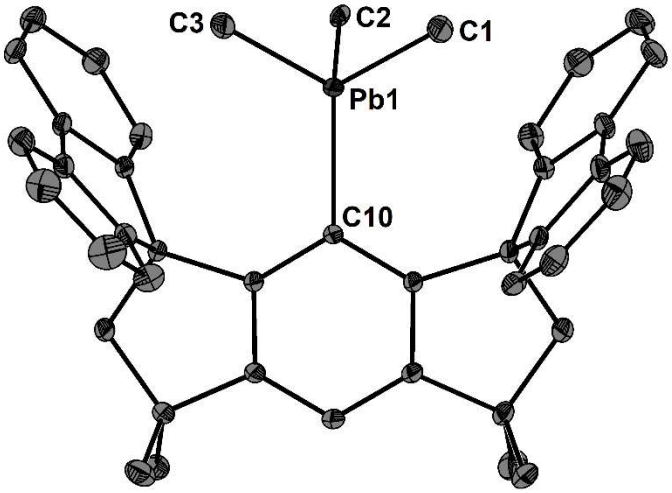

Figure S44. Molecular structure of **4** showing 50% probability ellipsoids and the essential numbering scheme. Selected bond lengths [Å]: Pb1-C1 2.225(2), Pb1-C2 2.310(1), Pb1-C3 2.224(2), Pb1-C10 2.254(2).

Computational Methods

Density functional theory (DFT) calculations (geometry optimizations in the gas-phase) were performed at the B3PW91/6-311+G(2df,p)[S12,S13] level of theory using Gaussian09.[S14] For the Sn and Pb atoms, an effective core potential (ECP28MDF)[S15] and corresponding cc-pVTZ basis set was utilized. For NMR calculations, the larger QZVP basis set was employed on the optimized geometries (single-point). Topological analysis of the electron density according to the Atoms-In-Molecules (AIM)[S16] space-partitioning scheme was conducted using AIM2000,[S17] whereas DGRID[S18] was used to generate and analyze the Electron-Localizability-Indicator (ELI-D)[S19] related real-space bonding descriptors (grid step size: 0.05 a.u.). The non-covalent interactions index (NCI)[S20] grids were computed with NCIplot.[S21] Bond paths are displayed with AIM2000,[S17] while ELI-D and NCI figures are displayed with MolIso.[S22] AIM bond topology exceeds the Lewis picture of chemical bonding as it also includes weak secondary interactions, such as C–H···H–C and E···C_π, which is not only relevant for packing motifs in crystal structures but also for intra-molecular interactions. AIM also provides atomic basins, giving access to atomic/fragmental charges and volumes. In contrast, ELI-D provides basins of paired electrons, giving access to electron populations and volumes of bonding or lone-pair sections. Together AIM and ELI-D thus facilitate the determination of minute charge rearrangements following structural changes. NCI uncovers (extended) regions in space where non-covalent interactions occur, thereby greatly complementing AIM and ELI-D. In effort to estimate the Lewis acidity, we calculated FIA, HIA and CIA values according to the methods of Greb et al. using Me_3SiX (X = F, H, Cl) als references including a COSMO solvation model (CH_2Cl_2).[29,30]

Table S4. Topologic and integrated AIM and ELI-D bonding indicators of E–C contacts.

contact or basin	d [Å]	d_1/d [%]	$\rho(r)$ [eÅ^{-3}]	$\nabla^2\rho(r)$ [eÅ^{-5}]	ε	$G/\rho(r)$ [a.u.]	$H/\rho(r)$ [a.u.]	N_{ELI} [e]	V_{ELI} [Å^3]	γ_{ELI}
1Si-I										
C2-Si	1.853	0.39	0.89	3.2	0.03	0.98	–0.73	2.45	8.9	1.96
C75-Si	1.835	0.39	0.91	3.0	0.07	0.97	–0.74	2.13	6.8	1.91
C79-Si	1.835	0.39	0.91	3.0	0.07	0.97	–0.74	2.45	8.9	1.96
C46-Si	2.985	0.48	0.10	0.5	1.25	0.41	–0.04			
C55-Si	2.985	0.48	0.10	0.5	1.25	0.42	–0.04			
1Si-II										
C2-Si	1.873	0.39	0.85	2.9	0.03	0.95	–0.72	2.40	8.7	1.97
C75-Si	1.846	0.39	0.89	2.8	0.05	0.96	–0.74	2.06	5.9	1.93
C79-Si	1.843	0.39	0.90	2.9	0.05	0.97	–0.74	2.07	6.1	1.93
C41-Si	2.362	0.42	0.31	–0.3	0.25	0.34	–0.41	0.60	2.1	1.35
1Ge										
C1-Ge	1.935	0.48	0.93	–0.4	0.07	0.61	–0.63	2.44	8.8	1.72
C75-Ge	1.916	0.48	0.95	–0.6	0.01	0.60	–0.64	2.13	6.9	1.66
C79-Ge	1.927	0.48	0.93	–0.7	0.00	0.59	–0.64	2.11	6.9	1.67
C34-Ge	3.008	0.48	0.10	0.6	0.68	0.44	0.00			
C54-Ge	3.007	0.48	0.10	0.6	0.69	0.44	0.00			
1Sn										
C1-Sn	2.125	0.51	0.75	2.3	0.10	0.66	–0.45	2.31	10.5	1.67
C75-Sn	2.116	0.52	0.75	2.1	0.02	0.64	–0.44	1.91	7.9	1.60
C79-Sn	2.123	0.52	0.74	2.0	0.03	0.63	–0.44	1.89	7.8	1.60
C34-Sn	3.064	0.50	0.11	0.8	1.71	0.48	–0.01			
C54-Sn	3.064	0.50	0.11	0.8	1.72	0.48	–0.01			
1Pb										
C1-Pb	2.204	0.54	0.71	2.0	0.12	0.60	–0.41	1.92	8.1	1.59
C75-Pb	2.202	0.54	0.70	1.8	0.05	0.58	–0.39	1.47	5.4	1.50
C79-Pb	2.208	0.54	0.70	1.8	0.05	0.57	–0.39	1.46	5.3	1.51
C34-Pb	3.123	0.51	0.11	0.9	2.05	0.55	0.04			
C54-Pb	3.123	0.51	0.11	0.9	2.05	0.55	0.04			

For all contacts, d_1 is the distance of the Si atom to the bond critical point (bcp), $\rho(\mathbf{r})_{bcp}$ is the electron density at the bcp, $\nabla^2\rho(\mathbf{r})_{bcp}$ is the corresponding Laplacian, ε is the bond ellipticity, $G/\rho(\mathbf{r})_{bcp}$ and $H/\rho(\mathbf{r})_{bcp}$ are the kinetic and total energy density over $\rho(\mathbf{r})_{bcp}$ ratios, N_{ELI} and V_{ELI} are electron populations and volumes of related ELI-D basins, γ_{ELI} is the ELI-D value at the attractor position.

Table S5. AIM atomic and fragmental charges (in e).

	Si I	**Si II**	**Ge**	**Sn**	**Pb**
E	2.69	2.68	1.57	1.55	1.22
R_{ind}	–0.30	–0.31	0.08	0.06	0.17
Me_1	–0.65	–0.65	–0.27	–0.26	–0.14
Me_2	–0.65	–0.65	–0.26	–0.25	–0.13
Σ	1.10	1.07	1.12	1.11	1.13

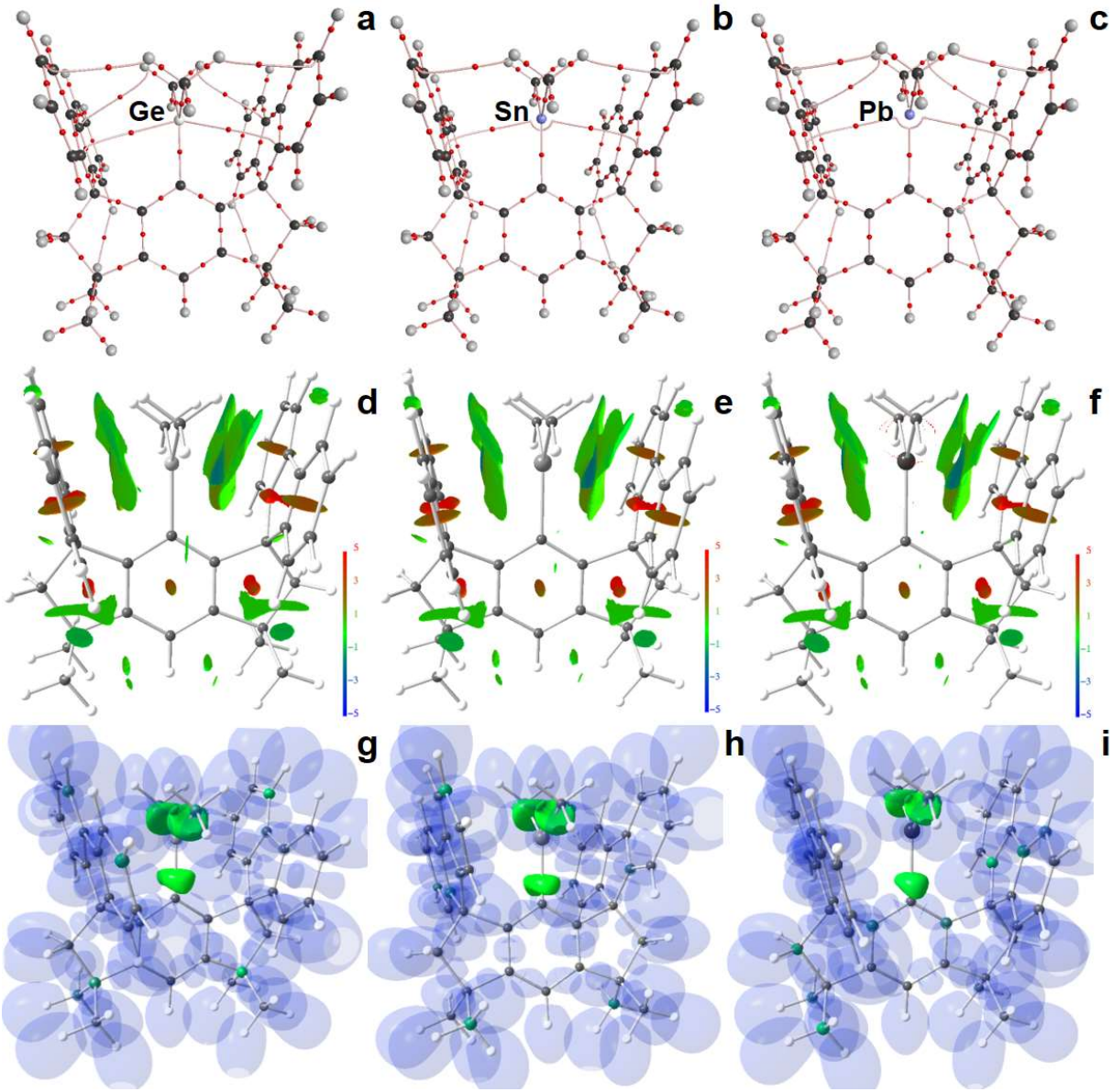

Figure S45. RSBI analysis of **1Ge** (left), **1Sn** (middle) and **1Pb** (right). (a-c) AIM bond paths motif, (d-f) NCI *iso*-surface at s(**r**) = 0.5, (g-i) ELI-D localization domain representation at *iso*-value of 1.3.

Table S6. Calculated ^{29}Si NMR-parameters on the B3PW91/QZVP-level.

	EMe_4	$[R_{ind}Me_2E]^+$		
model	shielding	shielding	anisotropy	delta
1Si-I	329.99	94.11	290.32	235.89
1Si-II	329.99	184.65	193.31	145.35

Table S7. Calculated HIA, FIA, and CIA values of solvated (CH_2Cl_2) cations **1Si**, **1Ge**, **1Sn** and **1Pb**.

model	E [a.u.]	ΔE [a.u.]	ΣE_1 [a.u.]	ΣE_2 [a.u.]	$\Delta E_{(2-1)}$ [a.u.]	$\Delta E_{(2-1)}$ [kJ mol^{-1}]	ΔE_{corr} [kJ mol^{-1}]
$SiMe_3$	-409.0539						
$SiMe_3H$	-409.8636	-0.8097					-451.7
$SiMe_3F$	-509.1808	-100.1269					-415.9
$SiMe_3Cl$	-869.5091	-460.4551					-287.4
1Si-I	-1913.4363						
1SiH	-1914.2084	-0.7721	-2323.2999	-2323.2623	0.0376	98.7	-353.0
1SiF	-2013.5174	-100.0812	-2422.6171	-2422.5714	0.0457	120.0	-295.8
1SiCl	-2373.8380	-460.4017	-2782.9453	-2782.8919	0.0534	140.3	-147.1
1Ge	-3700.9424						
1GeH	-3701.7070	-0.7646	-4110.8060	-4110.7609	0.0451	118.3	-333.4
1GeF	-3800.9961	-100.0537	-4210.1232	-4210.0500	0.0732	192.2	-223.7
1GeCl	-4161.3341	-460.3918	-4570.4514	-4570.3881	0.0634	166.3	-121.0
1Sn	-1838.3713						
1SnH	-1839.1175	-0.7462	-2248.2349	-2248.1714	0.0635	166.6	-285.1
1SnF	-1938.4106	-100.0393	-2347.5521	-2347.4645	0.0876	229.9	-186.0
1SnCl	-2298.7584	-460.3871	-2707.8803	-2707.8123	0.0680	178.6	-108.7
1Pb	-1816.9121						
1PbH	-1817.6442	-0.7321	-2226.7757	-2226.6981	0.0776	203.7	-247.9
1PbF	-1916.9333	-100.0212	-2326.0929	-2325.9872	0.1057	277.6	-138.3
1PbCl	-2277.2885	-460.3764	-2686.4212	-2686.3424	0.0787	206.7	-80.6

ΣE_1 sums up $SiMe_3X$ (X = H, F, Cl) and 1E(+) (E = Si, Ge, Sn, Pb); ΣE_2 sums up SiMe(+) and 1EX.

Additional References

[S1] M. Ito, D. Hashizume, T. Fukunaga, T. Matsuo, K. Tamao, *J. Am. Chem. Soc.*, 2009, **131**, 18024-18025.

[S2] M. Olaru, S. Mebs, J. Beckmann, *Angew. Chem. Int. Ed.*, 2021, **60***,* 19133-19138.

[S3] H. Gilman, R. G. Jones, *J. Am. Chem. Soc.* 1950, **72**, 1760-1761.

[S4] P. Romanato, S. Duttwyler, A. Linden, K. K. Baldridge, J. S. Siegel*, J. Am. Chem. Soc.* 2010, **132**, 7828-7829.

[S5] V. J. Scott, R. Çelenligil-Çetin, O. V. Ozerov, *J. Am. Chem. Soc.*, 2005, **127**, 2852-2853.

[S6] G. R. Fulmer, A.J.M. Miller, N.H. Sherden, H.E. Gottlieb, A. Nudelman, B.M. Stoltz, J. E. Bercaw, K.I. Goldberg, *Organometallics*, 2010, **29**, 2176-2179.

[S7] U. Mayer, V. Gutmann, W. Gerger, *Monat. Chem.*, 1975, **106**, 1235-1257.

[S8] M. Beckett, G. Strickland, *Polym. Commun*., 1996, **37**, 4629-4631.

[S9] V. Gutmann, *Coord. Chem. Rev.*, 1976, **18***,* 225-255.

[S10] O. V. Dolomanov, L. J. Bourhis, R. J. Gildea, J. A. K. Howard, H. Puschmann *J. Appl. Cryst.* 2009, **42**, 339-341.

[S11] K. Brandenburg, Diamond, version 4.0.4, Crystal Impact GbR: Bonn, Germany, 2012.

[S12] A. D. Becke, *J. Chem. Phys*. 1993, **98**, 5648-5652.

[S13] J. P. Perdew, J. A. Chevary, S. H. Vosko, K. A. Jackson, M. R. Pederson, D. J. Singh, C. Fiolhais, *Phys. Rev*. B 1992, **46**, 6671-6687.

[S14] M. J. Frisch, G. W. Trucks, H. B. Schlegel, G. E. Scuseria, M. A. Robb, J. R. Cheeseman, G. Scalmani, V. Barone, B. Mennucci, G. A. Petersson,; et al. *Gaussian09*, revision D.01; Gaussian, Inc.: Wallingford, CT, 2010.

[S15] (a) D. Figgen, G. Rauhut, M. Dolg, H. Stoll *Chem. Phys.* 2005, **311**, 227-244. (b) K. A. Peterson,; C. Puzzarini, *Theor. Chem. Acc*. 2005, **114**, 283-296. (c) B. Metz, H. Stoll, M. Dolg, *J. Chem. Phys.* 2000, **113**, 2563. (d) K. A. Peterson, *J. Chem. Phys.* 2003, **119**, 11099.

[S16] R.W.F. Bader, *Atoms in Molecules*. A Quantum Theory; Cambridge University Press: Oxford U.K., 1991.

[S17] F. Biegler-König, J. Schönbohm, D. Bayles, *J. Comput. Chem*. 2001, **22**, 545-559.

[S18] M. Kohout, *DGRID*-4.6 Radebeul, 2015.

[S19] M. Kohout, *Int. J. Quantum Chem.* 2004, **97**, 651-658.

[S20] E. R. Johnson, S. Keinan, P. Mori-Sanchez, J. Contreras-García, A. J.; Cohen, W. Yang, *J. Am. Chem. Soc.* 2010, **132**, 6498-6506.

[S21] J. Contreras-García, E. Johnson, S. Keinan, R. Chaudret, J.-P. Piquemal, D. Beratan, W. Yang, *J. Chem. Theor. Comp.* 2011, **7**, 625-632.

[S22] C. B. Hübschle, P. Luger, *J. Appl. Crystallogr*. 2006, **39**, 901-904.